Title

Physics-Based Failure Modeling of Manganese Dioxide Pseudocapacitors with Probabilistic Methods for Improved Lifetime Prediction and Energy System Operation

Author

Ndefru, Bineh Gese

Publication Date

2023

Peer reviewed|Thesis/dissertation

UNIVERSITY OF CALIFORNIA

Los Angeles

Physics-Based Failure Modeling of Manganese Dioxide Pseudocapacitors with Probabilistic Methods for Improved Lifetime Prediction and Energy System Operation

A dissertation submitted in partial satisfaction of the

requirements for the degree Doctor of Philosophy

in Materials Science and Engineering

by

Bineh Ndefru

2023

ABSTRACT OF THE DISSERTATION

Physics-Based Failure Modeling of Manganese Dioxide Pseudocapacitors with Probabilistic Methods for Improved Lifetime Prediction and Energy System Operation

by

Bineh Ndefru

Doctor of Philosophy in Materials Science and Engineering

University of California, Los Angeles, 2023

Professor Ali Mosleh, Co-Chair

Professor Bruce S. Dunn, Co-Chair

As we shift away from fossil fuel-derived energy and the electrification of various systems grows exponentially, society is increasingly relying on energy storage systems such as batteries to store and distribute energy on demand. While batteries are a widely studied technology, other energy storage technologies such as supercapacitors have unique performance qualities that can provide alternatives or supplements to batteries in systems. This dissertation delves into MnO2 pseudocapacitors, aiming to unravel the degradation mechanisms impacting their performance and reliability under diverse operating conditions, toward their usage (or other pseudocapacitive materials) in real systems. While there is a growing body of research on pseudocapacitors, including MnO2-based pseudocapacitors, little work has gone into frameworks for predicting

their behavior under various environmental and operating conditions. Through a multifaceted approach of experimental investigation, physics-based modeling, and probabilistic analyses, this research centers on elucidating the impact of temperature and degradation of active material on the aging of devices, ultimately predicting capacitance reduction over time.

Two approaches are taken in this research to predict end of life for pseudocapacitors. The first approach utilizes a first-principles physics model, augmented with Bayesian methods to integrate experimental and statistical information with uncertainties into the model. This method allows for the prediction of changes happening in the cell over numerous cycles, and the associated capacitance reductions. The second approach develops for the first time the use of a Bayesian Monte Carlo approach for estimating the remaining useful life (RUL) of pseudocapacitors based on experimental data with quantified uncertainty. The combination of estimates from these models can lead to improved prediction based both on real world experience through data and on theoretical knowledge of the system.

Overall, this dissertation advances the prediction of aging in MnO2 pseudocapacitors and develops models that can be applied to various other pseudocapacitive systems. These contributions lay a foundation for further exploration that may decrease the time required to conduct pseudocapacitor experiments and contribute to the management and longevity of energy storage systems containing pseudocapacitors.

The dissertation of Bineh Ndefru is approved.

Timothy S. Fisher

Yinmin Wang

Bruce S. Dunn, Committee Co-Chair

Ali Mosleh, Committee Co-Chair

University of California, Los Angeles

2023

Dedication

“To the world we dream about, and the one we live in now”.

Table of Contents

List of Figures viii
CHAPTER 1 1
1. Introduction 1
1.1. Motivation 1
1.2. Background 4
1.2.1. Energy Storage Mechanisms of Pseudocapacitors 4
1.2.2. Pseudocapacitor Aging and Degradation (Failure Modes and Mechanisms) 6
CHAPTER 2 11
2. Research Objectives and Contributions 11
2.1. Recent Advances in Supercapacitor Modeling 11
2.2. Objectives 13
2.3. Contributions 15
CHAPTER 3 18
3. Experimental Work and Characterization 18
3.1. Experimental Setup & Degradation Characterization 18
3.2. Degradation Characterization 20
3.3. Results 22
3.3.1. Microscopy 22
3.3.3. Cyclic Voltammetry 23
3.3.4. Ultraviolet Visible Spectroscopy 27
3.3.5. Electrochemical Impedance Spectroscopy 29
3.3.6. Self-Discharge and Leakage Currents 31
CHAPTER 4 33
4. Modeling of MnO_2 Electrodes in Aqueous Sodium Sulfate Electrolyte 33
4.1. Model Structure Overview 33
4.2. Physics-based Modeling of MnO_2 Pseudocapacitor 34
4.3. Physical Modeling of Aging Phenomena 38
4.3.2. Degradation modeling 38
4.3.3. Parameter Estimation 39
4.3.4. Parameter Estimation from Experimental Data 40
4.3.5. Bayesian Inference for Statistical Parameter Estimation and Updating 40
4.4. Model Results and Validation 44

4.5. Model Limitations 49
CHAPTER 5 51
5. Remaining Useful Life Prediction 51
5.1. Introduction 51
5.2. Probabilistic lifetime model 52
5.3. Model Determination for RUL Prediction 63
5.4. Integration with Physics-based Lifetime Model 68
5.4.2. Model Weighting Based on Uncertainty 68
5.4.3. Bayesian Model Uncertainty 69
5.5. Discussion 71
CHAPTER 6 73
6. Case Studies and Applications 73
6.1. Case Study 73
CHAPTER 7 76
7. Summary 76
7.1. Conclusions and Outlook 77
7.2. Future Work: Addressing Model Limitations and Advancing RUL Predictions 78
References 81

List of Figures

Figure 1. Ragone plot comparing energy and power densities for capacitors, batteries, and supercapacitors [3]. 2

Figure 2. (Left) Power requirements and timescales for various grid services, as compared to the energy storage options (right) that can deliver power on these time scales and at those power ratings [4]. 4

Figure 3. Schematic of charge transfer processes of redox reactions and intercalation pseudocapacitance into the bulk of electrodes, as compared to EDLCs and battery-like devices [7]. 5

Figure 4. Common failure mechanisms in supercapacitors [12]. 7

Figure 5. Failure Mechanisms, Modes, and Effects diagram for supercapacitors [13]. 10

Figure 6. SEM images of MnO2 electrode (left) as deposited and (right) after 1000 cycles of cyclic voltammetry. 23

Figure 7. (a) cyclic voltammogram of pseudocapacitive MnO2 in the first cycle and after 1000 cycles. (b) Plot of capacitance retention after 1000 cycles. (c) CV at 40C (d) capacitance retention at 40C 24

Figure 8. a-c) cyclic voltammograms of MnO2 pseudocapacitive devices at 20C, 40C and 50C respectively. d) Specific capacitance of the sample in (a), showing steadily increasing capacitance with cycling. e) plots of specific capacitance over cycles for 20C, 40C, and 50C. 26

Figure 9. Specific capacitance evolution with cycling of cell with annealed MnO2 electrode 27

Figure 10. a) UV-Vis spectra of 10 ml aliquots of electrolyte before cycling, after 10 cycles, and after 100 cycles. b) plot of concentration of MnO2 in electrolyte over cycles. 28

Figure 11. a-e) Nyquist plots showing various tests on samples at room temperature. f) Nyquist plot of sample at 40C 30

Figure 12. Plot of charge transfer resistance over the cycles tested, showing larger increases at lower cycles as compared to higher cycles. 31

Figure 13. Plots of leakage current over time, obtained at 20C, 40C, and 60C. 32

Figure 14. Overview of electrochemical model structure, highlighting the use of conditional probabilities for updating the behavior in each cycle and the interaction of the model with external data. 33

Figure 15. Schematic diagram of one-dimensional pseudocapacitor cell from [39] 35

Figure 16. Bayesian Belief Network used for parameter updating, showing the probabilistic relationships used to develop the conditional probability table. (in supplementary material). 41

Figure 17. Example of data used to estimate change in internal temperature per cycle. a) highlights an example of a value for ΔT that occurs within the 2nd cycle [82]. b) shows the slowing increase in temperature at high cycle numbers and the influence of current [85]. 42

Figure 18. Concentration profiles at the first cycle for a) the oxidant species and b) reductant species. Bottom: Concentration profiles at the 200th cycle for c) oxidant species and b) reductant species. 44

Figure 19. a) Voltage profiles for multiple scan rates from 5mV/s to 100mv/s. (b) Example of simulated CV results with faradaic current in red, capacitive current in yellow, and total current in blue. c) faster scan rate – 0.01 mV/s. d) slower scan rate – 0.001 mV/s. 45

Figure 20. Sensitivity analysis of various model parameters, each simulated while keeping all others constant. 47

Figure 21. a) 500 cycles (plotted every 50 cycles). b) Specific capacitance over cycles for the run in (a). c) 500 cycles plotted every 100 cycles..... 48

Figure 22. a) cycle 100 of a simulated cyclic voltammogram. b) cycles 1 and 100 of cyclic voltammogram for a real cell collected experimentally..... 49

Figure 23. Illustration of Markov Chain Monte Carlo process, with sampling from proposal distribution, and uncertainty propagated to posterior distribution in the form of a histogram. 54

Figure 24. Best fit surfaces for parameters a and b of exponential model. 61

Figure 25. a) Specific capacitance over 100 cycles at room temperature. b) Histogram of predicted RUL 64

Figure 26. Best fit surfaces for parameters a, b, and c in the power law model 67

Figure 27. EPA Urban Dynamometer Driving Schedule..... 74

Acknowledgements

I have immense gratitude for all the people who supported me through this journey. Thank you to my graduate advisor, Professor Ali Mosleh, for his support and guidance and for making the B. John Garrick Institute for the Risk Sciences (GIRS) feel like a welcoming place of learning and growth. I am grateful to have had the opportunity to work in an interdisciplinary space where there was encouragement to pursue my goals, even those outside of the norm for a scientist or engineer. Thank you for your patience and gentle push to keep pace toward completion of this degree, even through major setbacks including a pandemic. Thank you to the rest of my committee members, Professor Dunn, Professor Fisher, and Professor Wang, for their guidance and for sharing their time, expertise, and their resources with me.

Thank you to Professor Laurent Pilon for his personal and professional guidance early on in the process and the year of education and financial support through the NSF Traineeship--Innovations at the Nexus of Food, Energy, and Water Systems.

Thank you to all my colleagues in GIRS, among them, Joselyne Saldana, Arjun Earthperson, Dr. Marilia Ramos, Dr. Tara Parhizkar, and Dr. Wadie Chalgham. I'm grateful for not only the support of my research, but for the warm group environment created by all of you. Special thank you to Theresa Stewart and Karthik Sankaran for their support with understanding various complex topics and the countless hours working through technical problems with my research and the COVID-19 project.

Finally, I would like to thank so many people—partners, friends, family, co-conspirators, and ancestors—who made the completion of this dissertation possible. I cannot thank you enough for your support and encouragement. Thank you to my leadership team and friends in the Science Policy Group at UCLA for keeping my eye on the prize. Special thank you to my mom and

siblings for your unwavering support and belief in me, through this process and throughout my life, which helped me also believe that I could do it.

Vita

Education

2015 B.S. Engineering and Public Policy

B.S. Materials Science and Engineering

Carnegie Mellon University

Pittsburgh, Pennsylvania

Research & Work Experience

Graduate Student Researcher: Garrick Institute for the Risk Sciences, UCLA

Start Date: Jan. 2020; End Date: Dec. 2023 | Supervisor's Name: Ali Mosleh

Graduate Student Researcher: UCLA Labor Center

Start Date: Apr. 2023; End Date: Oct. 2023 | Supervisor's Name: Caroline Luce

Teaching Assistant: UCLA

Start Date: Jan. 2020; End Date: Dec. 2023 | Supervisor's Name(s): Ali Mosleh, Marilia Ramos, Audrey Pool-O'Neal

Summer Intern: RAND, Santa Monica, CA

Start Date: Jun. 2022; End Date: Sep. 2022 | Supervisor's Name(s): Yuliya Shokh, Brien Alkire

Post-Bachelors Researcher: Los Alamos National Laboratory

Start Date: Jul. 2016; End Date: Aug. 2018 | Supervisor's Name(s): Veronica Livescu, George Rusty Gray, Millicent Firestone

Energy Policy Intern: Center for American Progress

Start Date: May 2014; End Date: Sep. 2014 | Supervisor's Name: Miranda Peterson, Ben Bovarnick

Selected Publications

Ndefru, B., Sankaran, K., Stewart, T., Mosleh, A., Earthperson, A., Zawalick, N., "Risk-Informed Decision-Making Tool for Covid-19 Community Behavior and Intervention Scenario Assessment," *Probabilistic Safety Assessment and Management PSAM 16,* (2022)

Aggarwal, A., Cheung, C., **Ndefru, B.**, "Establishing Modern Grid Resilience in the Southeast United States," *Journal of Science Policy & Governance,* (2021).

Barr, K., Goldgerd, A., **Ndefru, B.**, Philson, C.S., Ryznar, E., Zweng, R., "Policy Memo: Water in Los Angeles: Rethinking the Current Strategy," *Journal of Science Policy & Governance,* (2020).

Ndefru, B.G., Ringstrand, B.S., Diouf, S.I.Y., Seifert S., Leal, J.H., Semelsberger, T.A., Dreier, T.A, Firestone, M.A., "Multiscale additive manufacturing of polymers using 3D photo-printable self-assembling ionic liquid monomers," *Mol. Syst. Des. Eng*. (2019).

Liu, Y., Cheng, P., Yuan, J., Huang, T., Wang, R., Meng, D., **Ndefru, B.G.**, Zou, Y., Sun, B., Yang, Y., "Enabling Efficient Tandem Organic Photovoltaics with High Fill Factor via Reduced Charge Recombination," ACS Energy Lett., (2019)

Livescu, V., Beyerlein, I.J., Bronkhorst, C.A., Dippo, O.F., **Ndefru, B.G.**, Capolungo, L., Mourad, H.M., "Microstructure insensitive twinning: A statistical analysis of incipient twins in high-purity titanium," *Materialia* (2019).

Jones, D.R., Fensin, S.J., **Ndefru, B.G**., Martinez, D.T., Trujillo, C.P., Gray III, G.T. "Spall Fracture in Additive Manufactured Tantalum," *Journal of Applied Physics* (2018).

Presentations

Ndefru B.G., Firestone, M., Livescu, V., Gray III, G.T., Valdez, J., (2018). *Mechanical Testing of a Nanostructured Lyotropic Mesophase Material from an Ionic Liquid Monomer*. Presentation at the annual Technical Materials Society Conference.

Ndefru, B.G., Fensin, S.J., Lienert, T., Knapp, C., Gray III, G.T., Pacheco, R., (2017). *Effects of Solidification Parameters in Additively Manufactured 304L Stainless Steel.* Presentation at the annual Materials Science and Technology Conference.

Awards

1. **Shine On Scholarship (2020)**
   -Scholarship from SolarCity and GivePower for one woman in STEM to attend the GREEN Program in Nepal to study Microgrids Systems for Rural Development at Kathmandu University and work in the mountain village of Solpathana.
2. **NSF Innovations at the Nexus of Food, Energy and Water Systems (INFEWS) traineeship (2019)**

CHAPTER 1

1. Introduction

1.1. Motivation

Worldwide, there is escalating demand for energy storage systems for a variety of uses. Electric vehicle sales are increasing exponentially in many regions of the world [1], requiring more innovation on the electrochemical energy storage (EES) systems that power them. Another pressing need is to increase the integration of renewable energy sources such as solar and wind into the power grid. Due to their inherent intermittency, these energy systems can cause destabilization to power grids that are already often unreliable and vulnerable. Blackouts across the United States are the result of weather events and equipment failures and have been estimated to cost $150 billion each year [2]. As climate change worsens, the grid is more susceptible to extreme weather events and more catastrophic blackouts are predicted to occur. Energy storage systems offer solutions to these challenges of intermittency and peak loads, enabling faster integration and better utilization of renewable energy sources on the grid while also enhancing the reliability of the aging power infrastructure, and resiliency to extreme events.

A subject of extensive research, EES is a versatile technology that converts stored chemical energy into electricity, finding a wide variety of applications from personal devices to utility level energy storage. Traditional EES, such as batteries, while effective, face limitations from relatively slow charging rates and short cycle life. Electrical double layer supercapacitors (EDLCs) are a type of EES and a compelling research pursuit due to their unique characteristics including high power density, long cycle life, rapid charging, high efficiency, and environmental friendliness, though they may suffer from lower energy density that batteries [3].

Pseudocapacitors (a type of supercapacitor) have emerged as a promising storage solution due to their ability to combine high energy and power density. The Ragone plot in Figure 1. indicates that pseudocapacitors have not only the ability to store more energy than capacitors or EDLCs, but can also offer higher power densities than batteries, a boon for applications that require fast charging and discharge, such as electric vehicles.

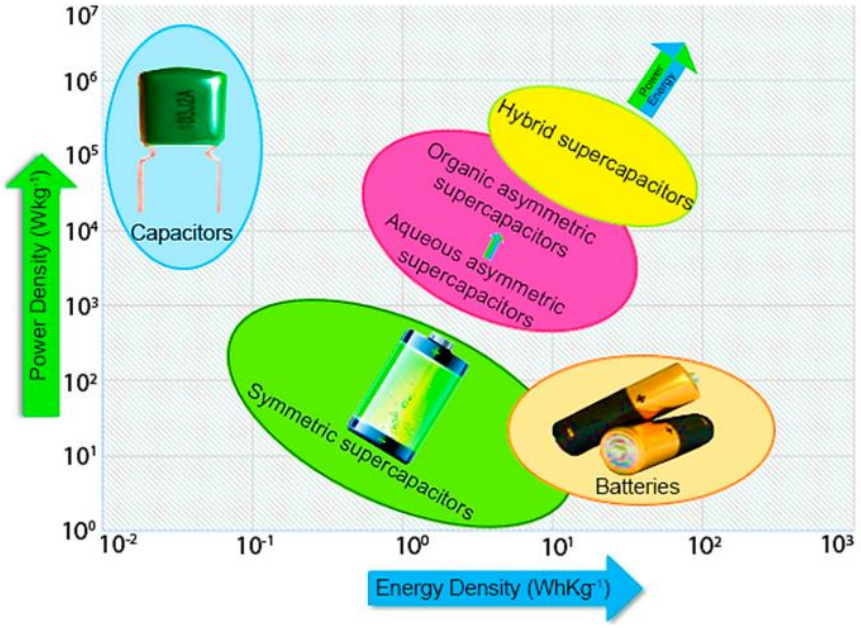

Figure 1. Ragone plot comparing energy and power densities for capacitors, batteries, and supercapacitors *[3]*.

One of the key advantages of pseudocapacitors lies in their ability to respond rapidly on the second-to-minute time frame, outperforming traditional batteries that typically respond in the minute-to-hour time frame or some mechanical energy storage systems that respond in the day-month time frame. This enables pseudocapacitors to efficiently address challenges related to power quality, intermittent balancing, load following, frequency response, voltage support, black start conditions, and avoid potential shutdowns (see Figure 2) [4]; or to recover more energy and

extend the life of electric vehicle batteries that face high discharge currents from regenerative braking, for example [5]. This rapid response capability makes pseudocapacitors particularly well-suited for dynamic operations, where real-time adjustments are required to maintain stability and reliability. Their versatility makes them potentially valuable assets for many energy systems.

To achieve reliability in complex systems like a power grid or an electric vehicle, it is necessary to achieve efficiency and reliability in the various components that support storage, conversion, and utilization of energy sources. Many researchers claim remarkable cycling stability (i.e. stability of capacitance and resistance values) of their pseudocapacitor devices, some on the order of 100,000 or more [6]. This far exceeds conventional batteries, most with cycle lives less than 1000 cycles. Despite these claims for some pseudocapacitors, cycle and calendar aging (including degradation that occurs when not in use) are difficult and often intractably long to determine for the wide variety of environmental and experimental conditions devices may be subject to. While there is novel research on pseudocapacitor physics, there is little work that aims for their utilization in critical systems by simulating and predicting how they may behave for these long periods of time under varying conditions. As pseudocapacitors become commercialized, understanding the physics and being able to accurately predict supercapacitor lifetime under real-world conditions is critical to the operation of systems and the people that they support. This research aims to enable system optimization and lifetime prediction with physics-based modeling and probabilistic modeling of pseudocapacitor behavior and degradation under different loads and environmental conditions.

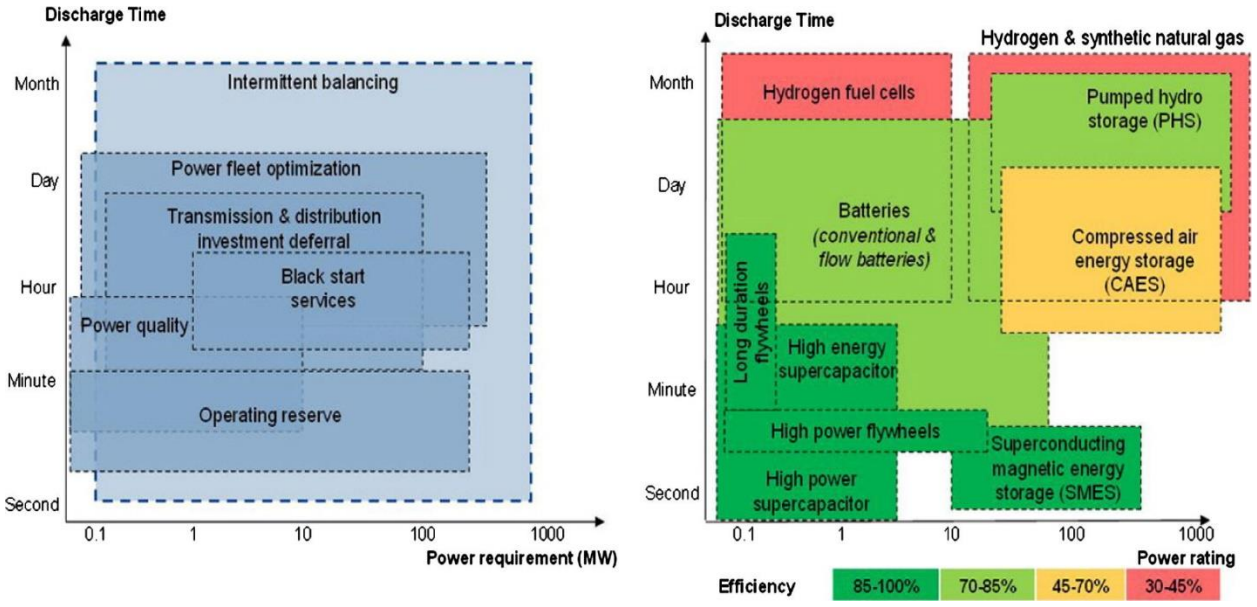

Figure 2. (Left) Power requirements and timescales for various grid services, as compared to the energy storage options (right) that can deliver power on these time scales and at those power ratings *[4]*.

1.2. Background

1.2.1. Energy Storage Mechanisms of Pseudocapacitors

Pseudocapacitors are able to achieve the charge/discharge rates and relatively high theoretical capacitance values that set them apart from batteries and EDLCs due to a unique combination of charge storage mechanisms. Capacitors store limited charge because the storage mechanism is electrostatic interactions that only occur near the surface of the electrode. Batteries store charge via bulk diffusion-limited processes that necessitate structural changes which impede the kinetics of the charge transfer process. Pseudocapacitors, however, undergo fast and reversible faradaic battery-like redox reactions at the surface of the electrode wherein charges are transferred, or intercalation in the bulk of the material due to ion channels in the structure of the electrode.

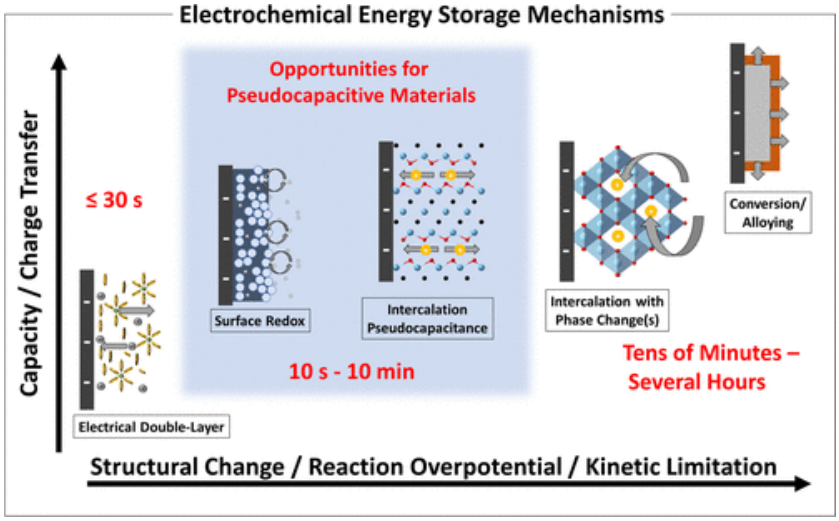

Figure 3. Schematic of charge transfer processes of redox reactions and intercalation pseudocapacitance into the bulk of electrodes, as compared to EDLCs and battery-like devices *[7]*.

Transition metal oxides such as ruthenium oxide (RuO_2), manganese oxide (MnO_2) nickel oxide (NiO), cobalt oxide (Co_3O_4) are commonly used as pseudocapacitor electrodes. Amorphous MnO_2 pseudocapacitive electrodes in sodium sulfate (Na_2SO_4) electrolyte are the focus of this study. The Mn and Na species involved undergo a redox reaction, wherein Mn is reduced and gains electrons, while Na is oxidized and loses electrons. The electron charge transfer is mediated by the transport of Na^+ to the surface of MnO_2 where the valence of Mn changes from Mn^{4+} to Mn^{3+} to Mn^{2+}. The reaction is shown in equation (1).

$$MnO_2 + Na^+ + e^- \leftrightarrow Na \cdot MnO_2 \quad (1)$$

Low electronic conductivity limits redox reactions to the surface of the electrode. Despite this, the theoretical capacity of MnO_2 is 308 mAh/g over a potential window of 0-0.9V. Bulk diffusion is thought to be the predominant influence on the performance, as compared to variations in surface area, due to high ion diffusion rates in various crystal structures that have been observed [8]. Amorphous MnO_2, however, is unlikely to have long range order that is thought to facilitate bulk ion diffusion. Therefore, it is assumed in this study that the reactions

are not intercalation reactions and have a greater dependence on surface area for the surface redox reactions. Because amorphous, however, the surface features structural defects that can enhance diffusion kinetics [9].

1.2.2. Pseudocapacitor Aging and Degradation (Failure Modes and Mechanisms)

Some researchers have reported cycling stability of MnO_2 pseudocapacitors up to 20,000 cycles [10]. Despite these successes and the claim of theoretical long life and long-term stability, supercapacitors often show pronounced performance degradation in operation [11]. Like EDLC materials which have been more widely studied Figure 4. Common failure mechanisms in supercapacitors , [13], [14] (see Figure 4), there are various failure mechanisms for pseudocapacitors. A common failure mode for pseudocapacitors is electrode material degradation, particularly in transition metal oxide-based pseudocapacitors like MnO_2 and RuO_2. During charge and discharge cycles, repeated redox reactions can lead to material degradation, resulting in the loss of active surface area and reduced capacitance over time. MnO_2 under the inappropriate conditions can be irreversibly reduced to lower valence products that produce soluble Mn^{2+} ions. The reaction in equations (2) and (3) shows the dissolution reactions for acidic and basic electrolytes respectively. [15]

$$Mn_2O_3 + 2H^+ \rightarrow Mn^{2+} + MnO_2 + H_2O \quad (2)$$

$$2MnOOH \rightarrow Mn^{2+} + MnO_2 + 2OH^- \quad (3)$$

Dissolution decreases the availability of active material for capacitance. This phenomenon is more severe at higher temperatures, larger surface areas, low electrolyte pH, and higher potentials [16, 17, 18]. The dissolved transition metal ions, however, can go through a subsequent process of redeposition on the positive electrode in various forms [19]. While many researchers report capacitance degradation with dissolution, Yang et al. [20] found that some

dissolved Mn^{2+} re-oxidizes to a birnessite-phase of MnO_2 and redeposits on the surface in a flower-like nanostructure. This new morphology and phase was an improvement on the interlayer spacing of the other ramsdellite phase present, suggesting a self-repairing process of dissolution and redeposition. Therefore, it seems possible to either achieve better or worse capacitance upon cycling MnO_2 depending on the starting phase of the material.

Studies on MnO_2 based electrodes have also reported morphological and structural changes that may impact cycling stability [21, 22]. Additionally, mechanical stress and volume changes during charge-discharge cycles can cause electrode delamination or cracking, leading to the formation of non-conductive regions and further capacity loss [12]. [23] suggests another route of mechanical degradation resulting from oxygen evolution and volumetric variation, leading to poor conductivity in manganese flakes/petals.

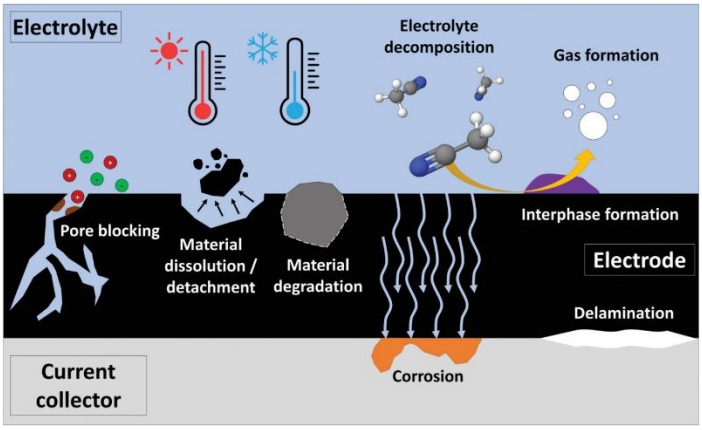

Figure 4. Common failure mechanisms in supercapacitors *[12]*

Self-discharge is another phenomenon that hinders the long-term performance and efficiency of pseudocapacitors. Self-discharge is the decrease in capacity from a spontaneous drop in voltage when the device is disconnected from an external circuit. This arises as the device goes back to

an equilibrium state, wherein non-equilibrium charge carriers in the electrolyte and electrode recombine since electronic charges can no longer pass through an external circuit [24, 25]. This causes unwanted side-reactions and parasitic processes, involving slow ion migration and chemical reactions at the electrode-electrolyte interface. While batteries also experience self-discharge, pseudocapacitors experience self-discharge to a greater degree, in some cases experiencing a 10% loss of stored energy within an hour [25]. Improving the self-discharge characteristics of pseudocapacitors is an important area of research. While many experimentalists conduct consecutive cycles from which to build lifetime models, a robust lifetime model should account for this mechanism that occurs on the calendar life rather than the cycle life scale and inhibits these devices from making headway in real applications. While it may not pose a problem for connected systems with intermittent recharge (such as electric vehicle regenerative breaking), the inability to maintain capacity would be impractical for systems in which they are required to remain on standby.

Another failure mechanism arises from electrolyte degradation. Over extended cycling or high temperatures, the electrolyte can undergo chemical breakdown, resulting in the formation of side products and gas evolution. These processes may lead to an increase in the cell's internal resistance, reducing charge transfer efficiency and overall capacitance. As with electrolyte degradation, temperature plays a significant role in influencing supercapacitor performance and failure at the separator, electrodes together decreasing the lifespan of the device by 50% for every 10°C above their working temperature [26]. While increasing temperature can increase capacitance under certain conditions [27], extreme temperatures beyond a threshold can accelerate aging and decrease performance, increase self-discharge rates, and affect the overall

safety and reliability of the device [28]. However, while batteries can experience dangerous thermal runaway, tests have shown no exothermic reaction leading to thermal runaway in EDLCs [26].

Figure 5 displays the various potential pathways to the failure of supercapacitors. Failures are defined as capacitance loss, increase in equivalent series resistance, or mechanical deformation of a cell. To mitigate these failure mechanisms, modes and effects, comprehensive research is required that supports better understanding of the underlying degradation pathways. Moritz Teuber suggests that it is important to connect first principles physics investigations to observable characteristics like capacitance loss to have a more complete assessment of operating conditions on performance and lifetime [29]. With better understanding of the degradation pathways, modelers may suggest optimal operating strategies that can improve the performance and extend the lifespan of pseudocapacitors, making them more viable for energy storage applications.

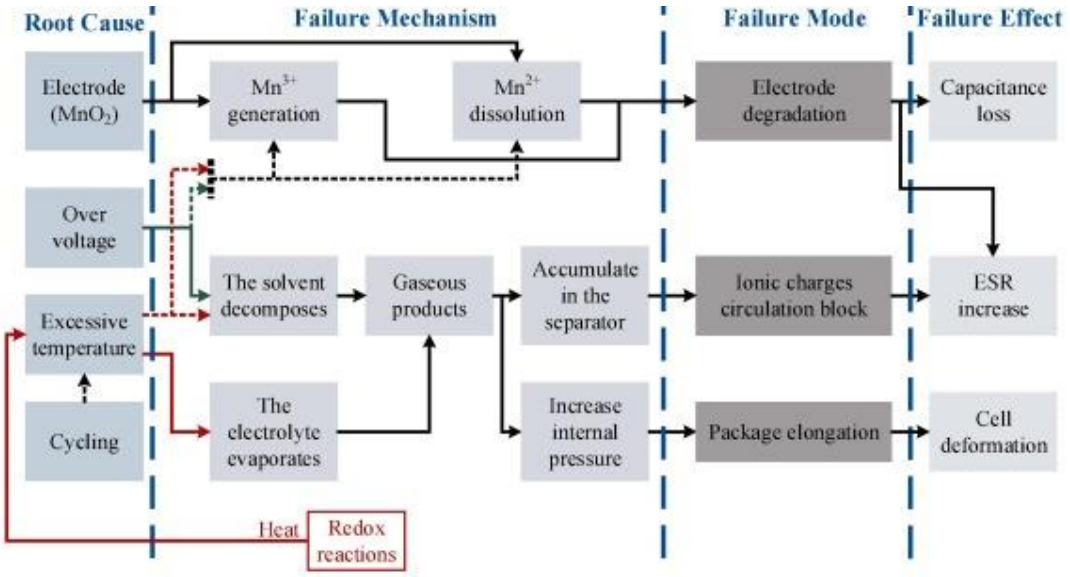

Figure 5. Failure Mechanisms, Modes, and Effects diagram for supercapacitors *[13]*.

Chen et al. [11] presented a review of modelling approaches for assessing aging and degradation of supercapacitors. Many of the papers reviewed are not interested in the reasons for performance degradation, and therefore use electrical modeling. However, these models are only valid at the beginning of a supercapacitor lifetime and can't accurately understand the lifetime effects of cycling under different conditions. Ma et al. [30] summarized modeling of supercapacitors and their aging. Their summary of electrochemical models suggests that while they have high possible accuracy, parameter measurement is not always possible so they cannot reflect the dynamic processes of charge/discharging and degradation. Through their reviews of models, [31] and [32] suggest the overall value of modeling these systems with accurate lifetime and reliability predictions by proposing the use of these models to determine key requirements for real supercapacitor management in vehicles or other systems. In the present work, the use of probabilistic methods along with electrochemical modeling combine to improve both understanding and prediction of behavior and are a step toward their use in systems.

CHAPTER 2

2. Research Objectives and Contributions

2.1. Recent Advances in Supercapacitor Modeling

As indicated by the various reviews on supercapacitor modeling, models can help elucidate the degradation mechanisms that are not readily measurable. This literature review covers various approaches to modeling the behavior of supercapacitors, with a particular focus on cyclic voltammetry (CV) curves, as they are one of the most informative characterizations of electrode processes. [33], [34], [35], [36] [37] adopted first principles electrochemical models to analyze EDLCs. These studies achieved significant milestones by providing analytical solutions for EDLCs, but pseudocapacitors were not covered. Some researchers [38], [39], [40], [41], [42], [43], [44] have simulated pseudocapacitive electrodes, but none have attempted to capture the evolution of degradation in the material over its lifetime. Carvalho et al. [45] similarly endeavor to predict and model the electrochemical response of pseudocapacitive cobalt hydroxide electrodes through CV curves. Although they achieved a representation of the faradaic redox behavior shape, the accurate representation of reactions occurring at electrodes (e.g., charged species in the electrolyte, diffusion phenomena) remained challenging. Nevertheless, these papers highlight the potential for improved diagnostics and lifetime analysis through first principles and CV curve modeling of supercapacitors.

Various other papers, such as [46], [47] utilize equivalent circuit models rather than first principles to simulate EDLC CV curves. Omori et al. [48] similarly model the degradation of EDLCs through the impedance on an equivalent circuit model. These equivalent circuit approaches approximate the processes in a pseudocapacitor to the components of a circuit. They

often necessitate fitting the models to large sets of experimental data for resistance and capacitance values and does not allow for proper diagnostics of degradation processes. Other work including [49] presents alternative methods, such as galvanostatic approaches, and explores physics-based methods to account for specific effects on EDLCs, such as mesopore effects. Other alternative methods include a state of health estimation method for EDLCs based on deep learning networks and Bayesian optimization [50] . Challenges concerning interpretability and limited data availability are noted, emphasizing the need for further data collection and exploration of Bayesian approaches. Another model of EDLCs uses machine learning for degradation models of capacitance outside of manufacturer specified temperature ratings validated on 9 commercial cells [51]. This, like many machine learning models can suffer from a lack of interpretability and that a physics-based model would not.

It is crucial to emphasize that none of the models for pseudocapacitors mentioned thus far have addressed the impact of external and changing internal temperatures, as well as the coupled effects of other stressors on degradation and capacitive behavior of pseudocapacitors. Pilon et al. [34] mention that measuring external temperature oscillations can underestimate the internal temperature, which may be very high near electrodes due to Joule heating which can lead to premature and unexpected degradation. Especially in high power applications, high cell temperatures can be generated. These excessive temperatures can cause accelerated aging, increased self-discharge, and decomposition of the electrolytes [52]. d'Entremont et al. developed a first principles thermal model of the Joule heating effect, faradaic reactions, and double-layer formation in pseudocapacitors [35]. Their model successfully captured the physical phenomena governing the thermal behavior of pseudocapacitors. However, their model does not

account for the impact of this internal temperature evolution on degradation over the cycle life. Moreover, while some work has been done for EDLCs [53], none have attempted to model the evolution of degradation over the cycle life of pseudocapacitors. In addition, the current models, while useful for assessing charge storage mechanisms and design, have not yet attempted to predict the remaining useful life (RUL) based on operating and environmental conditions. RUL and state of health are useful measures to provide decision support for the operation of pseudocapacitors in real systems. This research aims to fill these gaps and contribute to a more comprehensive understanding of pseudocapacitor behavior and performance.

2.2. Objectives

1. **Identify the Degradation Mechanisms of MnO_2 Pseudocapacitors under Different Operating Conditions**

   The first objective of this research is to investigate the degradation mechanisms that influence the performance and reliability of MnO_2 pseudocapacitors under varying operating conditions. This study focuses on the dissolution of the electrode material into the electrolyte as a mechanism that leads to capacitance reduction. Through experimental studies, modeling, and statistical analyses, the aim is to identify the key factors contributing to the extent of this degradation mechanism, such as temperature, cycling, and electrolyte pH. By investigating these mechanisms and the conditions under which they occur, this work seeks to develop an understanding of optimal operating conditions that would enhance the longevity of pseudocapacitors and systems that they may be a part of, e.g., electric vehicles.

2. **Develop a Model that Simulates the Capacitance and Degradation Behaviors of Pseudocapacitors over Time**

   To achieve a deeper understanding of pseudocapacitor behavior, a physics-based model is developed that simulates cyclic voltammetry of a pseudocapacitor device, simulating the degradation behaviors and the evolution of capacitance over time. This model incorporates factors such as the external and internal temperature over numerous cycles as they impact the changes in capacitance and the evolution of degradation.

3. **Improve upon Physics-Based Model Using Bayesian Updating and Validate the Proposed Model through Experimental Studies Conducted on Pseudocapacitor Devices**

   Bayesian updating of parameters in each cycle and time step of the model are employed to incorporate experimental and statistical data with uncertainties, enhancing the model's robustness and predictive capabilities for real operating conditions. By iteratively incorporating observed degradation patterns, the model can adapt and become more accurate in predicting pseudocapacitor performance over time. Experimental studies are also used to validate the proposed model's accuracy.

4. **Probabilistic Remaining Useful Life Prediction**

   Using a reliability engineering approach, this research also aims to demonstrate the applicability of a probabilistic model in predicting the Remaining Useful Life (RUL) of pseudocapacitors. By forecasting the RUL based on experimental data, the optimal

operation and management of pseudocapacitor energy storage systems can be inferred for varying environmental conditions. It can lend itself to maximizing the system availability and the lifetime of other components of a larger system, such as the batteries in an electric vehicle. By incorporating probabilistic analyses, the model can calculate and propagate the uncertainty of inputs, to a distribution of solutions with a measured confidence level. This lends itself to proactive maintenance and efficient utilization of pseudocapacitors, ultimately reducing downtime and minimizing the risk of system failure. This has not been done for pseudocapacitors before. Further, the comparison and ensemble results of the physics-based model and the probabilistic model of degradation can together provide more confident estimates.

In summary, this dissertation seeks to advance the understanding of MnO_2 pseudocapacitor degradation, develop a robust physics-based model using Bayesian updating, and demonstrate its value in predicting RUL and optimizing system operation. The research will contribute valuable insights into the performance of pseudocapacitors, with broader implications for enhancing the overall performance of energy storage systems in the pursuit of sustainable and dependable power solutions.

2.3. Contributions

Bringing together the fields of electrochemistry, materials science, and reliability engineering, this research introduces a hybrid model that integrates first-principles physics with Bayesian probabilistic approaches to model and predict pseudocapacitor behavior. The few existing pseudocapacitor models do not attempt to model the change in the behavior of the system from one cycle to the next. Modeling the electrochemical mechanisms and changes that occur over

long cycling durations would benefit researchers with faster exploration of materials under varying conditions. Unlike many other models, the model in this study utilizes existing data and experimental insights to provide a comprehensive understanding of pseudocapacitor degradation behavior (via active material dissolution) under various operating and environmental conditions over the cycle life. For example, joule heating is cited as a source of reversible and irreversible heat generation caused by the resistance of the material, which can impact the electrochemical reactions and the rates of dissolution and redeposition. By incorporating underlying physical mechanisms like these, the model is highly tunable and interpretable, while enabling prediction and suggesting strategies for optimal operation.

Probabilistic methods are not often employed to model electrochemical devices, especially pseudocapacitors. In this research, the physics-based model is integrated with probabilistic methods. While this has been done with batteries, these methods have not been applied to pseudocapacitor devices. The use of probabilistic methods allows for refined model inputs and an assessment of the stochastic nature of real electrochemical processes with quantified uncertainty, as opposed to deterministic outputs of typical physics-based models. The incorporation of Bayesian adjustment to the model presents an example that can also be applied to other existing supercapacitor models in the literature, leading to improved accuracy and reliability in their predictions.

Further, this study represents the first endeavor to probabilistically predict the reliability and Remaining Useful Life (RUL) of pseudocapacitors. This can facilitate the creation of Degradation Based Optimization models for larger system optimization and management. This

integration of first-principles physics and Bayesian probabilistic methodologies expands the state of knowledge, enabling more informed decision-making in materials and systems design, better reliability assessment for energy storage applications.

CHAPTER 3

3. Experimental Work and Characterization

3.1. Experimental Setup & Degradation Characterization

The electrochemical behavior of MnO_2 pseudocapacitors was examined by cyclic voltammetry (CV), one of the most informative characterizations of electrode processes. In a three-electrode setup, the resulting current is recorded as a function of changing potential over time. The current-voltage curves obtained through CV characterization allow for the study of the kinetics of electrochemical reactions, the measurement of device capacitance, the reversibility/irreversibility, and information about the capacitive behavior and faradaic redox reactions occurring at the electrode-electrolyte interface.

To prepare the MnO_2 test electrodes for CV, the following procedure was followed:

- Substrate Preparation—A conducting carbon cloth with dimensions of 1x2 cm^2 was cut and plasma cleaned to be the substrate for electrodeposition. The carbon cloth provides a conductive surface for the deposition of MnO_2. The cut samples were weighed on a microbalance before electrodeposition.
- Electrodeposition Process—A 0.1 M manganese acetate solution was prepared as the electrolyte for the electrodeposition process. The conducting carbon cloth was immersed in the manganese acetate solution, such that a 1x1 cm2 area was submerged. A constant current of 5 mA/cm^2 was applied for 20 minutes to facilitate the deposition of MnO_2 on the surface of the carbon cloth to be the working electrode for subsequent CV testing. Other researchers have found 20 minute deposition to be optimal for high performance of

their devices [54]. The samples were dried overnight and weighed again to assess the initial mass loading of active material on the substrate.

- Heat Treatment—The electrodes were tested both as deposited in their amorphous form (as confirmed by X-ray diffraction) and following a 6-hour heat treatment at 350°C as it was thought that treatment may reduce the propensity for Mn dissolution into the electrolyte. [55] suggests heat treatment of MnO_2 at this temperature leads to higher capacity and power outputs due to the structural conversion. Others, however, have found no change at 350°C from the amorphous material as-synthesized, and rather saw the development of short-range order resulting in mainly Mn^{3+}, with Mn^{4+} at the interior and Mn^{2+} at the surface [56]. This could, in fact, be detrimental to the electrode capacity due to the solubility of Mn^{2+} in Na_2SO_4 electrolyte.

For the CV experiments, the following materials were utilized:

- Carbon Cloth/MnO_2: served as the working electrode, where the electrochemical reactions occurred.
- Carbon Paper: used as the counter electrode to complete the electrochemical circuit and facilitate the charge transfer during CV.
- Ag/AgCl Reference Electrode: provided a stable reference potential for measuring the voltage applied to the working electrode.
- 1 M Aqueous Na_2SO_4 Electrolyte: ion conducting medium for the electrochemical reactions.

A three-electrode setup was chosen to explore the electrochemical properties of MnO_2 pseudocapacitors. A symmetrical set up is not necessary given that symmetrical MnO_2 devices have been shown to only undergo redox reactions at the negative electrode due to their high oxidation state and inability to be further oxidized at the positive electrode [57]. CV measurements were conducted at 1 mV/s, 5 mV/s, and 10 mV/s. The voltage window was selected to cover a range from 0 V to 0.8 V, ensuring the exploration of the desired potential range for the redox reactions without undergoing irreversible reactions around the electrolyte's decomposition limit (approximately 1.2 V for solutions in water due to the hydrogen and oxygen evolution reactions that cause gas bubbles and can also lead to mechanical degradation of the electrodes) [58, 59].

3.2. Degradation Characterization

For electrochemical energy storage technologies like batteries or supercapacitors, failure is typically when the device reaches 70-80% of nominal capacity [53]. In this study, high temperatures and elevated float voltage levels and scan rates were the variable stressors. The devices were subjected to numerous charge and discharge cycles while controlling the relevant parameters of voltage, scan rate, and temperature, and continuously evaluating the shapes of the cyclic voltammograms and the degree of capacitance fade, a key indicator of degradation. Because the dissolution of Mn compounds into the electrolyte is expected as a mechanism of this capacity fade, Ultraviolet-Visible Spectroscopy (UV-Vis) was used to measure the concentration change of materials in the electrolyte during cyclic voltammetry. Aliquots of electrolyte were taken at 5 cycles, 10 cycles, 20 cycles and/or at the end of cycling to measure the change in

absorbance after a certain amount of cycling. The change was then calculated to an average Mn loss per cycle in each regime (e.g., average loss per cycle within 0-20 cycles, or within 20-100 cycles).

The pH of the electrolyte was also confirmed to be neutral. Work by [60] and [61] suggested the association of pH with changing Mn^{2+} concentrations in electrolyte mixtures, with low pH leading to higher dissolution of active material. Further, [61] indicates that the overpotential for oxidation by MnO_2 has a dependence on pH, wherein neutral and basic conditions result in different mechanisms for water oxidation by manganese oxides.

Self-discharge and Electrochemical Impedance Spectroscopy (EIS) measurements were also taken. For self-discharge, the samples were charged, then held at a constant high voltage at the maximum of the voltage window for 30 minutes. Aliquots were then taken to examine in UV-vis. This was done at room temperature, 40C and 60C. Impedance measurements were taken intermittently before CV cycling, after 5 cycles, 10 cycles, and 20 cycles. These tests were also conducted at room temperature and the elevated temperatures.

High temperature testing of pseudocapacitors was employed to get an initial assessment of the performance of pseudocapacitor devices under different operating conditions. ALT is designed to expedite the assessment of a device's lifetime by subjecting it to intensified stress conditions. In this case, the increased stress conditions were higher temperatures (30, 40, 50, 60°C), and lower or higher scan rates. This accelerates aging processes and enables observation of failure modes and mechanisms in shorter times. The extrapolation of failure data using Arrhenius equations and acceleration factors can allow statistical prediction of device behavior and expected lifetime

under normal conditions without much knowledge of the system. Further, it allows direct understanding of behavior at higher stress conditions.

3.3. Results

3.3.1. Microscopy

SEM characterization shows imperfect adherence of the MnO_2 to the surface of the fibers of the carbon cloth and some cracking in the as deposited condition. After 1000 cycles, the SEM images show petal-like formations on the surface of the MnO_2 electrode. Given the findings of [61], [62], [63] , it is possible that these morphological changes are due to a dissolution-redeposition process that may happen as the Mn products of various oxidation states reduce or oxidize.

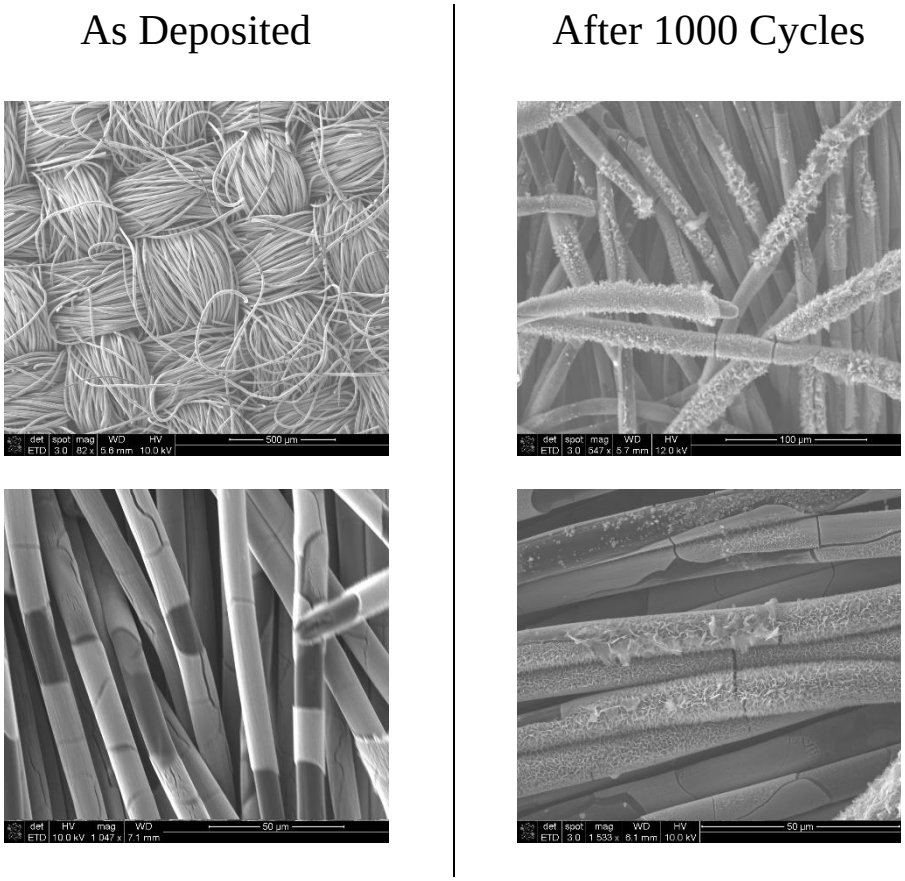

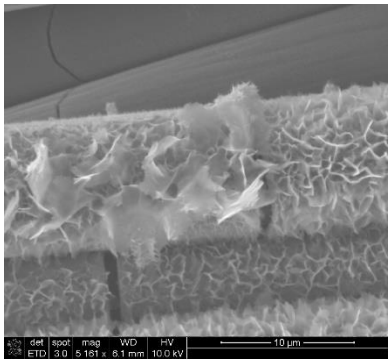

Figure 6. SEM images of MnO2 electrode (left) as deposited and (right) after 1000 cycles of cyclic voltammetry.

3.3.3. Cyclic Voltammetry

Cyclic voltammetry of a pseudocapacitive MnO_2 sample in

Figure *7* a and c shows a decrease in overall area of the CV curve after 1000 cycles suggesting a decrease in capacitance. After 1000 cycles, the CV also displays more pronounced redox peaks in

Figure *7*a. While the initial capacitance is larger for the sample cycled at elevated temperature of 40C (

Figure *7*c), the capacitance retention after 1000 cycles (

Figure *7*d) is lower than that of the sample cycled at room temperature.

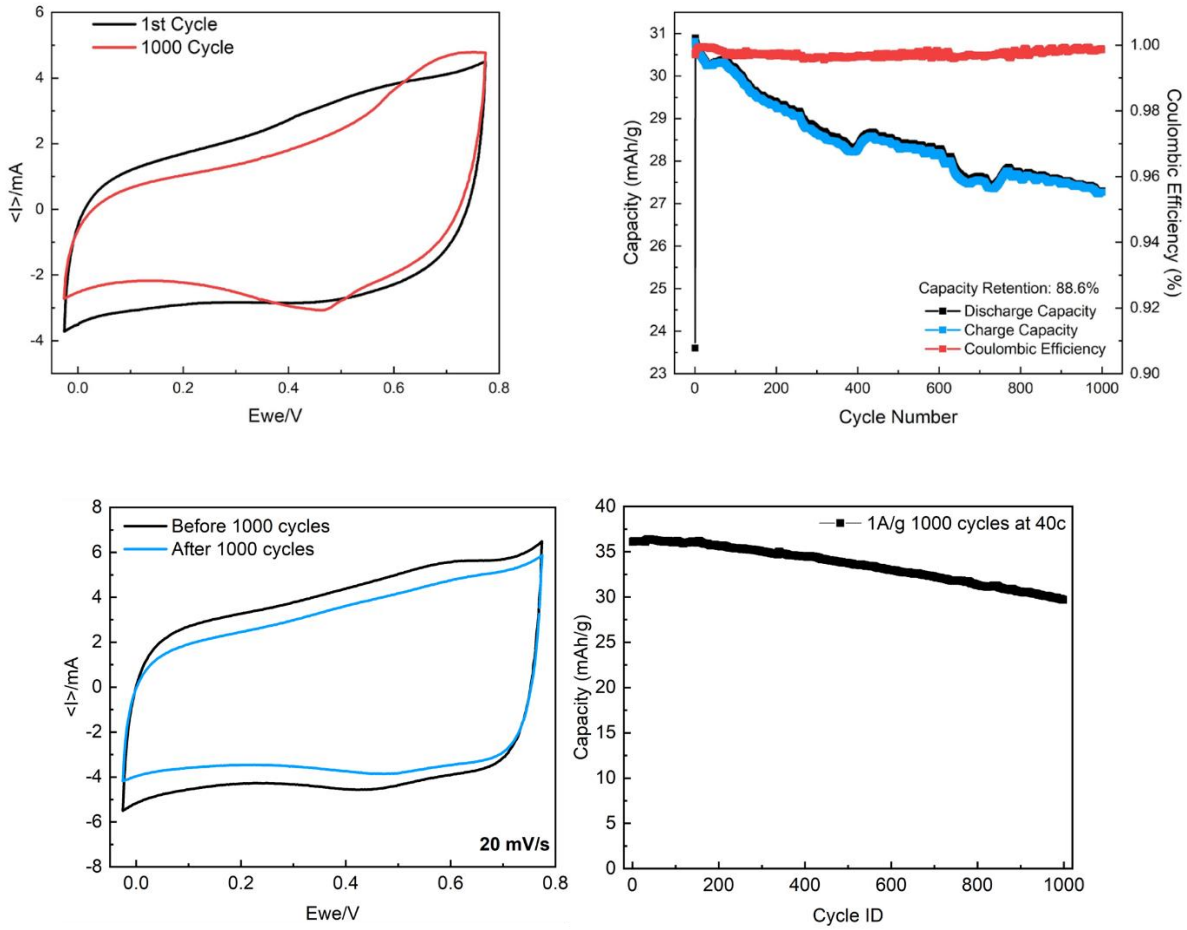

Figure 7. (a) cyclic voltammogram of pseudocapacitive MnO_2 in the first cycle and after 1000 cycles. (b) Plot of capacitance retention after 1000 cycles. (c) CV at 40C (d) capacitance retention at 40C

Figure 8, a-c, compares the cyclic voltammetry results of samples tested at 20°C, 40°C, and 50°C for 100-200 cycles. As the temperature increases, there is a noted shift in the shape of CV curves. At higher temperatures the shape departs from the rectangular shape to a more leaf-like shape, similar to the changes documented to occur with increasing scan rate in EDLCs and pseudocapacitors [64, 65, 66]. In each case, the capacitance calculated (Figure 8, e.) from the area of the CV curve shows an increase from initial values. Some researchers have suggested an electrochemical activation process in the initial cycles [67, 68, 69]. Given the surface area

dependence for capacitance, it is possible that this activation process is evident through the morphological changes seen upon cycling in Figure 6, which may give rise to more active sites for redox reactions, increased ion diffusion, and more surface area for double layer capacitance. This would align with researchers claims that the dissolution process is accompanied by a redeposition of the material back onto the electrode. This activation process appears to occur faster in samples tested at elevated temperature (Figure 8, e.) stopping around 25 cycles, while room temperature samples activation process ceases around >100 cycles. More characterization is necessary to assess the onset of these morphological changes, and how they impact the capacitance of the device. The final specific capacitance does, however, begin to decrease from the max value obtained after the initial activation process (as shown in Figure 8, e.). From the max values, samples tested at 40 and 50 °C exhibit a 97% capacitance retention and an 82% capacitance retention respectively.

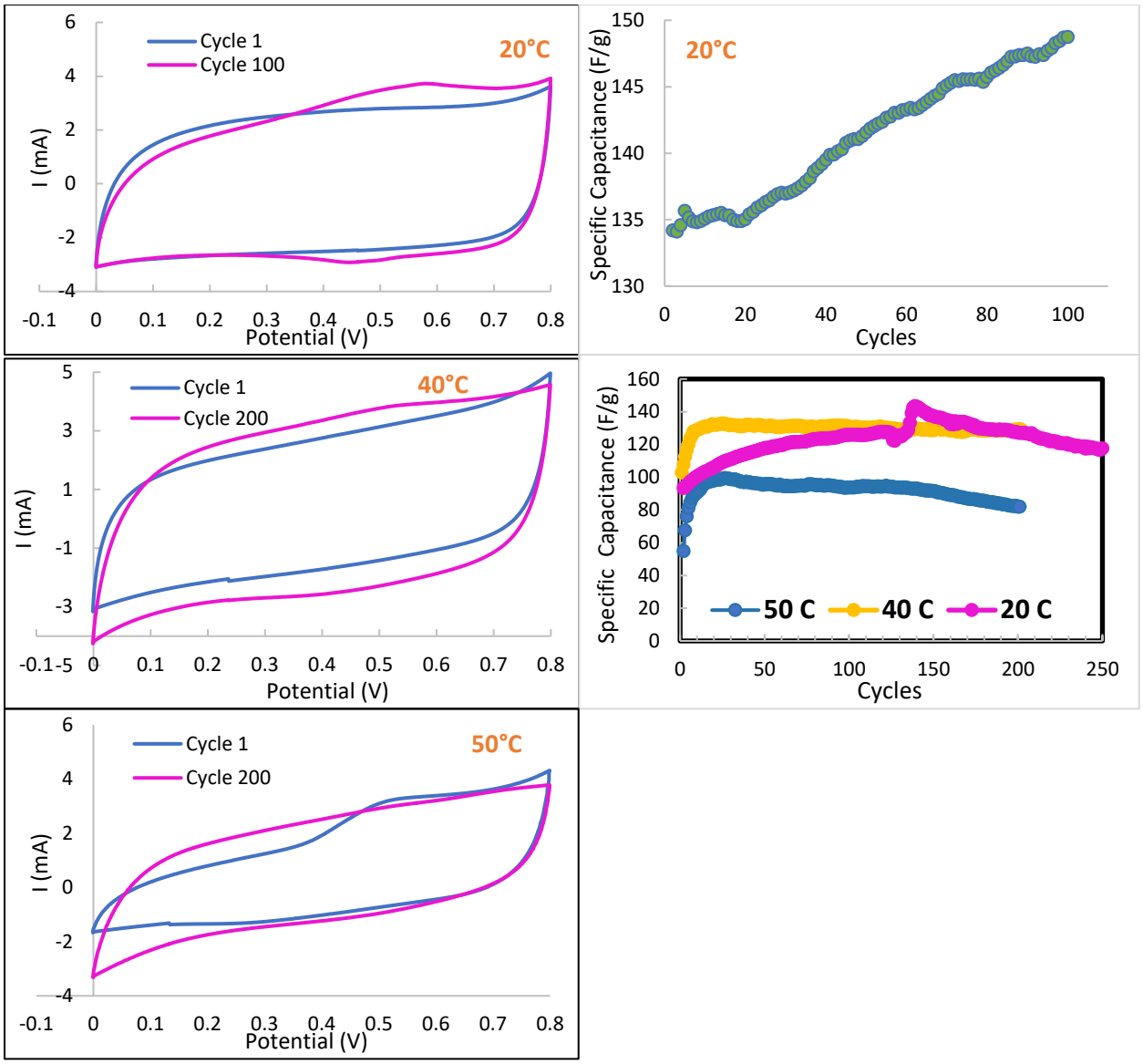

Figure 8. a-c) cyclic voltammograms of MnO2 pseudocapacitive devices at 20C, 40C and 50C respectively. d) Specific capacitance of the sample in (a), showing steadily increasing capacitance with cycling. e) plots of specific capacitance over cycles for 20C, 40C, and 50C.

Cyclic voltammetry of heat treated MnO_2 electrodes tested at room temperature in sodium sulfate resulted in relatively low specific capacitance values and a sharp decrease from initial values upon cycling (Figure 9). This is further evidence of the findings from [56] which found short-range order resulting in mainly Mn^{3+}, with Mn^{4+} at the interior and Mn^{2+} at the, a potential detriment to the electrode capacity due to the solubility of Mn^{2+} in Na_2SO_4 electrolyte.

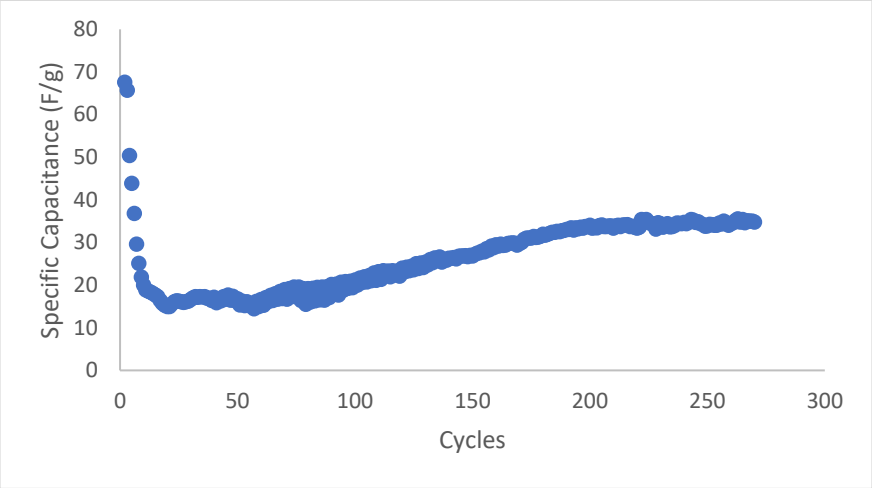

Figure 9. Specific capacitance evolution with cycling of cell with annealed MnO2 electrode

3.3.4. Ultraviolet Visible Spectroscopy

Because the dissolution of Mn compounds into the electrolyte is expected as a mechanism of this capacity fade, Ultraviolet-Visible Spectroscopy (UV-Vis) was used to measure the concentration change of materials in the electrolyte during cyclic voltammetry. Aliquots of electrolyte were successively taken from the three-electrode setup at various intervals of cycling. Based on the intensity of light through the sample solution, data for absorbance as a function of wavelength were obtained. The heights of the absorption peaks are directly proportional to the concentration of the species in solution, as described by the Beer-Lambert Law (equation (4)).

$$C = \frac{A}{\varepsilon \cdot d} \tag{4}$$

The sample concentration, C, depends on the absorbance, A, the distance of the light path, d, and ε, a material specific constant describing its molar absorptivity. The molar absorptivity of Mn2+ was determined to be 5.21E3 at a wavelength of 400 nm and that of MnO2 has been determined to be approximately 15000 [dm3.mol-1.cm-1] at a wavelength of 390 nm [70, 71, 72]. This measurement was done especially for conditions that were not represented by data in literature

[73, 74, 75, 76], i.e. mass or concentrations changes of Mn in electrolyte when cycling at high temperatures. Estimates were made of concentration increase per cycle (at lower cycle numbers and higher cycle numbers) and these values for the expected change in concentration per cycle were used in the electrochemical model in Chapter 5. Figure 10b shows the quick increase in active material concentration in electrolyte in early cycles relative to the slower increase in concentration in later cycles. The electrolyte solution tested was consistently neutral, though various papers suggest increased dissolution in acidic electrolytes [77, 78].

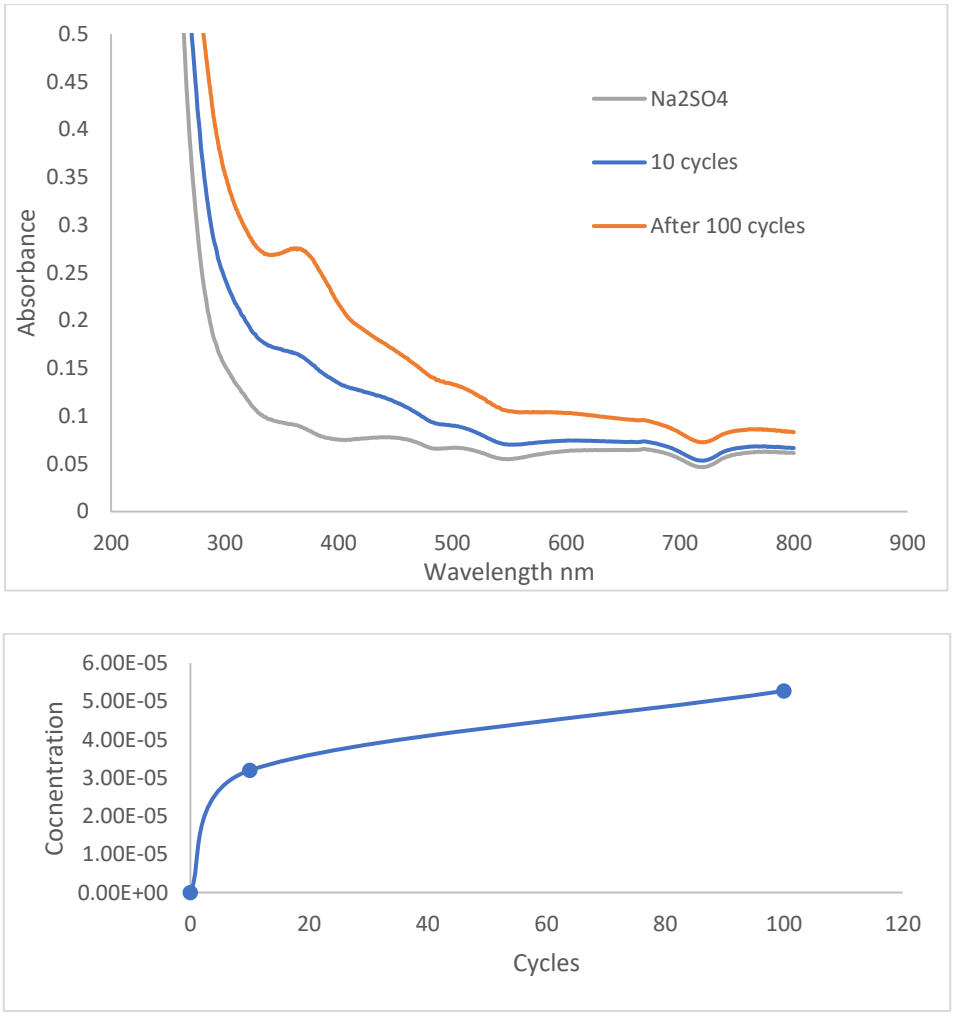

Figure 10. a) UV-Vis spectra of 10 ml aliquots of electrolyte before cycling, after 10 cycles, and after 100 cycles. b) plot of concentration of MnO2 in electrolyte over cycles.

3.3.5. Electrochemical Impedance Spectroscopy

Equivalent series resistance (ESR), charge transfer resistance (R_{CT}), and charge transfer rates were obtained from electrochemical impedance spectroscopy (EIS). Results of these tests for 20 and 40 °C are shown in Figure 11. Results of these tests conducted at 0, 5, 10, and 20 cycles indicate increasing resistance values upon cycling. An average increase in resistance per cycle, with a dependence on the temperature, was calculated from these results to be used in the electrochemical model. In each case, the resistance increases significantly from 0 to 5 cycles, and again between 5 and 10 cycles. Relative to these values, increases in resistance occurring between 10 and 20 cycles are minimal Figure 12. When tested at elevated temperature, while the ESR value slightly increased with cycling, the R_{CT} was seen to decrease slightly from initial values (Figure 11, f).

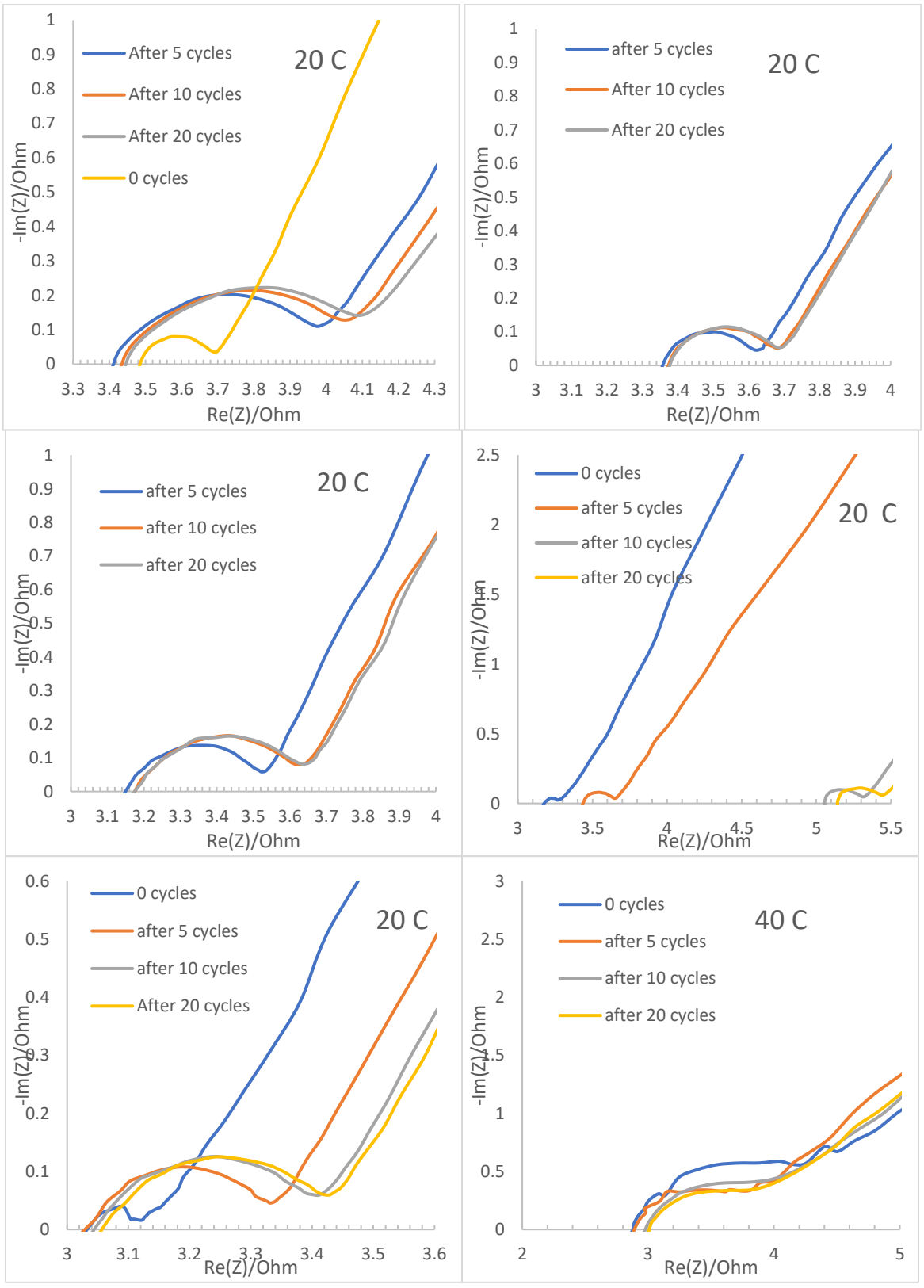

Figure 11. a-e) Nyquist plots showing various tests on samples at room temperature. f) Nyquist plot of sample at 40C

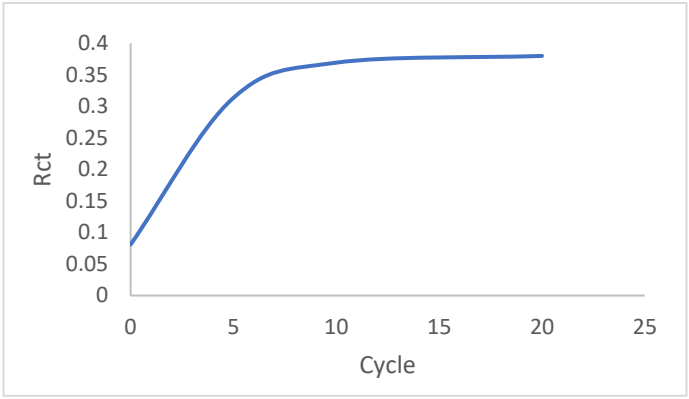

Figure 12. Plot of charge transfer resistance over the cycles tested, showing larger increases at lower cycles as compared to higher cycles.

These results are relevant to understanding the change in internal temperature occurring at each cycle, as the irreversible heat, the Joule heat, is a result of the internal resistance [79].

3.3.6. Self-Discharge and Leakage Currents

The self-discharge characteristics of MnO_2 pseudocapacitors were also assessed under different temperatures to provide insight into the stand-by performance and shelf life of devices. By observation alone when connecting to terminals of the potentiostat, the open circuit voltage of devices often started around 0.4 to 0.5 V and quickly declined. Within 10-20 minutes, the open circuit voltage often decreased to approximately 0.1 V or less. If left overnight after charging and reconnected the next day, the open circuit voltage would often be around -0.2 to 0.1 V.

A constant voltage test was conducted to quantify leakage currents, the parasitic current required to hold a supercapacitor at a charge at the rated voltage. The cells were charged and the voltage was set to the nominal voltage of the device, 0.8 V (given by the potential window within which

CV tests were conducted) and the current was measured over time. This current is the self-discharge current, the amount supplied by the DC source to maintain a given cell at a constant voltage and state of charge. The initial high current seen in Figure 13 is a result of ions reaching active sites of the material, while the stable current over time is the leakage current. Results of these tests at 20, 40, and 60 °C are shown in Figure 13. The leakage currents for cells tested at elevated temperature stabilize around approximately the same leakage current value of 30 mA. Room temperature samples stabilized around approximately 10 mA.

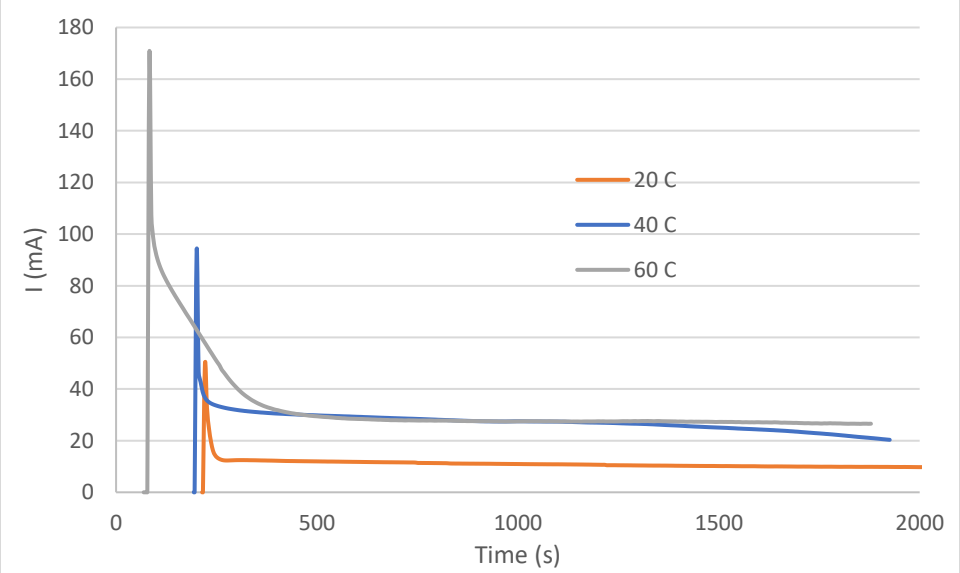

Figure 13. Plots of leakage current over time, obtained at 20C, 40C, and 60C.

CHAPTER 4

4. Modeling of MnO_2 Electrodes in Aqueous Sodium Sulfate Electrolyte

4.1. Model Structure Overview

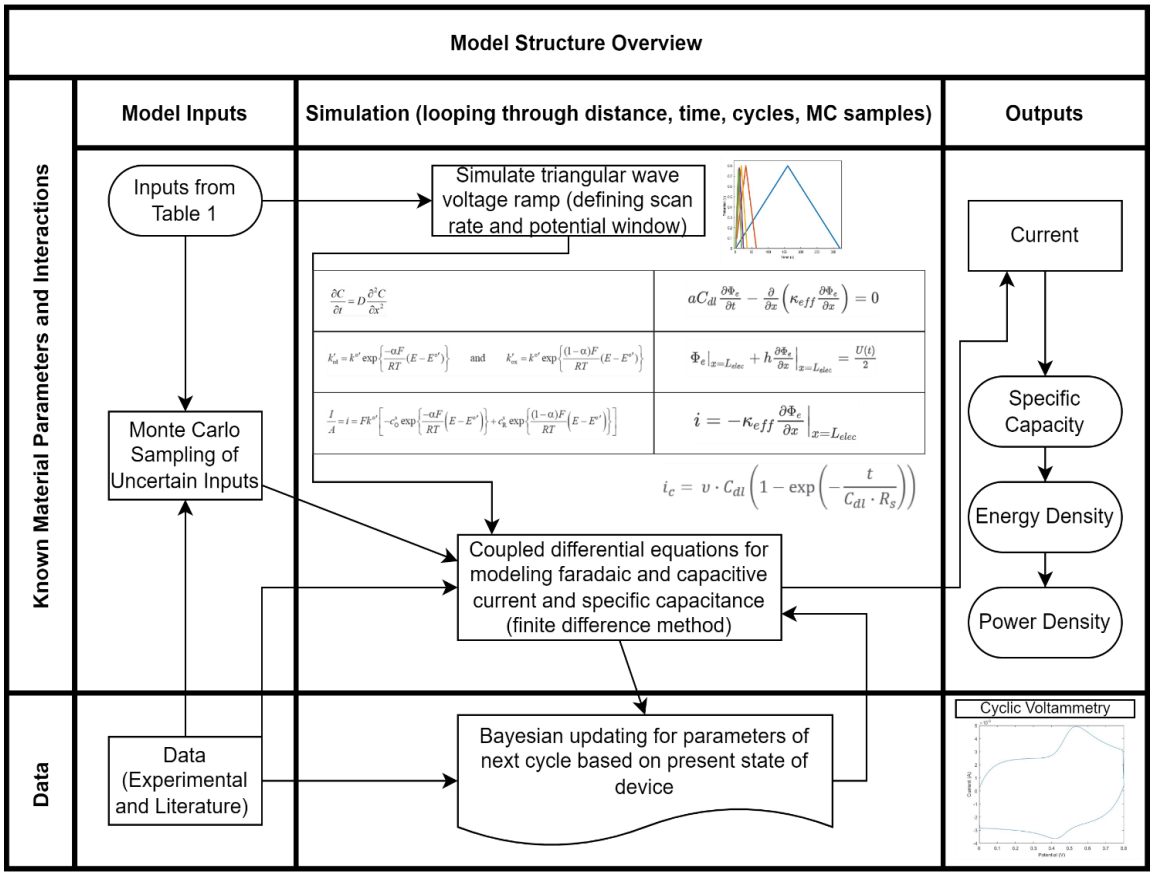

Figure 14. Overview of electrochemical model structure, highlighting the use of conditional probabilities for updating the behavior in each cycle and the interaction of the model with external data.

A physics-based model of pseudocapacitor behavior was developed in MATLAB. The model iteratively updates in time, distance, and cycle number with parameters informed by probabilistic methods that use variables from literature and from experiments that elucidate the degradation

processes occurring in redox-active MnO_2 pseudocapacitors. The outputs from the hybrid physics and probabilistic degradation model will then be used, along with data on the number of cycles to failure, to predict the remaining useful life (RUL) of the pseudocapacitor under various imposed conditions.

4.2. Physics-based Modeling of MnO_2 Pseudocapacitor

The objective for modeling pseudocapacitors is to understand and predict performance, aging and degradation, to guide experiments, and to support the optimization, scale-up and commercialization of the technology. This model seeks to model the charge and discharge process as it evolves in CV, wherein a linear voltage sweep is applied at a constant rate and the current response is the output. The fast and reversible redox reactions at the surface occurring in equation (1) are responsible for the faradaic current density, while the capacitive current results from the double-layer and does not involve chemical reactions.

Example model parameters are shown in

Table 1. The integral of the area in the modeled current-voltage profile is the specific capacitance (C_{sp}) of the device. The energy density (E_d in Wh/kg) and power density (P_d in W/kg) are derived from this (equations (5), (6), and (7))

$$C_{sp} = \frac{\int_{v1}^{v2} iV\, dV}{mv\Delta V} \tag{5}$$

$$E_d = \frac{1}{2} \times C_{sp} \times \Delta V^2 \tag{6}$$

$$P_d = \frac{E}{\Delta t} \tag{7}$$

In these equations, i is current, V is the voltage, and t is time.

The physics-based model at the continuum mechanics level was created in MATLAB. It is adapted from [80], [39], [45] and is schematically similar to the one-dimensional hybrid pseudocapacitor cell studied by [39] with a different electrolyte composition (Figure 15). The theoretical foundations of this model are the set of modified Poisson-Nernst-Planck (PNP) equations that describe ion diffusion and transport, specifically the effects of temperature, electric potential, or other variables on the ion concentrations as functions of space and time.

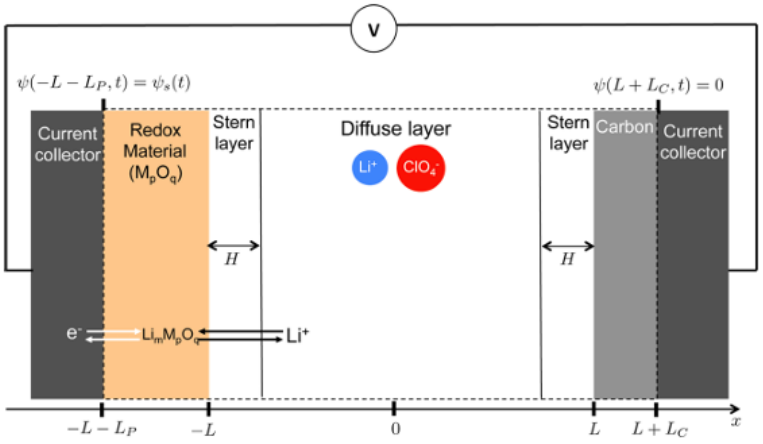

Figure 15. Schematic diagram of one-dimensional pseudocapacitor cell from *[39]*

This model uses a finite difference method with nested loops for spatial and temporal discretization to solve the partial differential equations that describe the diffusion of ions based on concentration gradients given by Fick's 2nd Law (equation 8) and calculate the flow of current at the electrode-electrolyte interface.

$$\frac{\partial C}{\partial t} = D \cdot \frac{\partial^2 C}{\partial x^2} \tag{8}$$

The empirical solution for the capacitive current (based on averages of double layer capacitance from experimental data) is calculated within the time loop, while the solution for the faradaic current is calculated both spatially and temporally. The currents estimated at each potential value simulate a CV cycle and are used to calculate the energy storage capacity of the simulated

pseudocapacitor. For a pseudocapacitor, the total current density, j_{tot} the sum of the current densities arising from capacitive charge transfer and faradaic charge transfer as in equation (9).

$$j_{tot} = j_c + j_f \tag{9}$$

$$j_c = -\kappa_{eff} \frac{\partial \phi_e}{\partial x}\Big|_{x=L} \tag{10}$$

$$j_f = j_0 \left[\exp\left(\frac{\alpha n_e F \eta}{RT}\right) - \exp\left(\frac{-(1-\alpha) n_e F \eta}{RT}\right)\right] \tag{11}$$

Here, κ_{eff} is the effective electrical conductivity of the electrolyte in the porous electrode, ϕ_e is the electric potential of the electrolyte, x is distance, α is the charge transfer coefficient, F is Faraday's constant, n_e is the number of electrons, and η is the overpotential (the difference between $\psi(t)$ and ψ_{eq}).

The approach of De Levie and other researchers [33] was used to calculate the capacitive current using the electric potential of the electrolyte ϕ_e within a porous electrode, given that the woven carbon fiber substrate creates a porous electrode. This satisfies a non-stationary diffusion equation (12) with initial condition (13)$\phi_e|_{t=0} = 0$ (13) and boundary conditions (14) and (15).

$$aC_{dl} \frac{\partial \phi_e}{\partial t} - \frac{\partial}{\partial x}\left(\kappa_{eff} \frac{\partial \phi_e}{\partial x}\right) = 0 \tag{12}$$

$$\phi_e|_{t=0} = 0 \tag{13}$$

$$\frac{\partial \phi_e}{\partial x}\Big|_{x=0} = 0 \tag{14}$$

$$\phi_e|_{x=L} + h \frac{\partial \phi_e}{\partial x}\Big|_{x=L} = \frac{U(t)}{2} \tag{15}$$

For the faradaic charge transfer process, the Butler-Volmer equation above (11) can break down into the oxidative and reductive portions of the reaction, represented by the charge transfer rates, k, for both processes (equations (16) and (17) respectively).

$$k'_{ox} = k_0 \exp\left(\frac{\alpha n_e \eta F}{RT}\right) \tag{16}$$

$$k'_{red} = k_0 \exp\left(\frac{-(1-\alpha) n_e \eta F}{RT}\right) \tag{17}$$

k_0 is the charge transfer rate constant. These charge transfer rates depend exponentially on the changing overpotential, η. Concentration gradients of the active material create diffusion gradients near the electrode surface that vary spatially and temporally. These gradients impact the rate of chemical reactions described by the Butler-Volmer equations. Therefore, numerical methods are required to solve the coupled partial differential equations. The boundary and initial conditions for the system are as shown in equations (18) – (21) [45].

$$c_{ox}\,(x, 0) = c_{ox}(L, t) = \; c_{ox,bulk} \tag{18}$$

$$c_{red}\,(x, 0) = c_{red}(L, t) = \; c_{red,bulk} \tag{19}$$

$$c_{ox}\,(x, 0) = \; c_{ox,surface} \tag{20}$$

$$c_{red}\,(x, 0) = \; c_{ox,surface} \tag{21}$$

A finite difference method was used to discretize the spatial and temporal domains of the modeled pseudocapacitor. The concentration changes of the oxidant and reductant are approximated at discrete grid points over time intervals. The flux is then calculated as:

$$j_{ox} \; = \frac{k_{ox} c_{ox}(1\Delta x, t) - k_{red} c_{red}(1\Delta x, t)}{1 + \frac{k_{ox}\Delta x}{D_{ox}} + \frac{k_{red}\Delta x}{D_{red}}} \tag{22}$$

By solving the system of equations iteratively, the method allows for the simulation of the time-dependent evolution of redox reactions during the charging and discharging process for a given cycle. The equilibrium potential is also adjusted in time as in [40]:

$$\Delta\Psi_{eq} = 10.5\left(4 - \frac{c_{1p}(t)}{c_{1p,max}}\right) - 39.9$$

The model computes these partial differential equations for each cycle and outputs the CV profile and the calculated specific capacitance. Due to the expectation of Mn dissolution as seen in literature and experimental results, the model accounts for degradation in the current-voltage characteristics of the pseudocapacitors CV profile by adjusting the amount of active material available for redox reactions from one cycle to the next. Further the model accounts for empirically determined changes in resistance during cycling. Given the uncertainty in temperature and ion concentrations, these values are sampled from uniform distribution and the model is run through as many cycles as the user is interested in assessing, for as many Monte Carlo samples as specified.

Table 1. Example parameters for electrode and electrolyte for physics-based simulation

Parameter	Value	Units
T – Temperature	variable	K
Area	2	cm^2
k_0 – Reaction rate constant	1.2E-1	$cm^{2.5}\,mol^{-0.5}s^{-1}$
α – Transfer coefficient	0.5	
υ – Scan Rate	0.005	mV/s
D – Diffusion Coefficient (bulk)	1E-5	cm^2/s
D_{ox} – Oxidant diffusion coefficient	5.27E-5	cm^2/s
D_{red} – Reductant diffusion coefficient	2.23E-4	cm^2/s
Ψ_{eq} – Equilibrium potential	0.5	V
Ψ – Applied Potential	0-0.8	V
c_{ox} – concentration of oxidant (Mn)	variable	mol/cm^3
c_{red} – concentration of reductant (Na)	variable	mol/cm^3
m – Active material mass	2.2	g/cm^2
pH	7	
Cycle number	variable	
Resistance	variable	$Ohms/cm^2$
Experimental steady state current mean	0.0025	Amps
x_{total} – total x range	$6\sqrt{D_{ox} * t_{cv}}$	cm
t_{cv} – total scan time	$2 * \frac{\Psi_{window}}{\upsilon}$	seconds

4.3. Physical Modeling of Aging Phenomena

4.3.2. Degradation modeling

Most existing models of pseudocapacitors aim to reproduce what occurs in a single charge and discharge cycle. A physics-based model that can correctly model how degradation evolves over time and multiple cycles requires knowledge of what parameters are changing, how they interact, and how they change from time step to time step. While there is not an easily applicable theoretical formula for how dissolution evolves in a pseudocapacitor, for example, data from various experiments can suggest how specific parameters of the model should change based on the conditions of the model at a given time step. In the present model of an MnO_2 pseudocapacitor, many model input parameters are obtained from literature that are simple point estimates or sampled from a fitting distribution of possible values (see Table 1). The parameters that impact the degradation in capacitance from one time step to the next are uncertain parameters that may not be easily calculated or measured at every time step. They therefore depend probabilistically on the condition of the model at a given time. These parameters include the internal/interface temperature, and the concentration of Mn products in the electrolyte.

4.3.3. Parameter Estimation

Point estimates or distributions of input parameters are determined based on experimental observations and from literature values. A normal distribution is then used to simulate the variation in possible values with the point estimate as the mean. A value for each parameter is selected using Monte Carlo random sampling. This is done for important operating parameters that are stochastic in nature (e.g., external temperature) and the samples are assigned to different time steps in a process similar to [81]. This is repeated multiple times for each parameter with

many random samples input to the physics model, allowing the model to generate not just a point estimate for the output capacitance, energy density, and power density values, but a distribution for the value after each charge/discharge cycle. This might allow a researcher or operator to estimate the best- and worst-case scenarios for their device, especially when experimentation is not a possibility.

4.3.4. Parameter Estimation from Experimental Data

The semi-empirical formulation of the model uses the double layer capacitance and changing resistance values obtained from experiments. Bard and Faulkner define the average steady state current value (where the current in the CV is approximately steady) as equal to $\upsilon \cdot C_d$, the scan rate times the double layer capacitance. Experiments allows estimation of this value with uncertainty to be used in the model. The results of EIS in section 3.3.5 permit the estimation of the change in resistance from one cycle to the next with uncertainty.

4.3.5. Bayesian Inference for Statistical Parameter Estimation and Updating

The identification and estimation of latent model parameters is important to understanding their impact on degradation. In this study, Bayesian inference is employed within the algorithm using measured data and literature to estimate and update the probability density functions (PDFs) of these parameters that are difficult to observe or unobservable (e.g., material loss percentage and internal temperature as shown in Figure 16). Instead of using a single fixed value for internal temperature or for dissolution amounts in the physics-based model, this method allows for probabilistic calculations that considers multiple possible internal temperature values based on their respective probabilities, given the input values of external temperature, current, cycle number, or pH at a given time in the model. This Dynamic Bayesian Network (DBN) in Figure 16 captures the complexity of the interactions of input parameters to the latent variables over

time. This is achieved with conditional probability tables (CPTs) that use data from literature, expert judgement, and best guesses for the mean values of the latent variables.

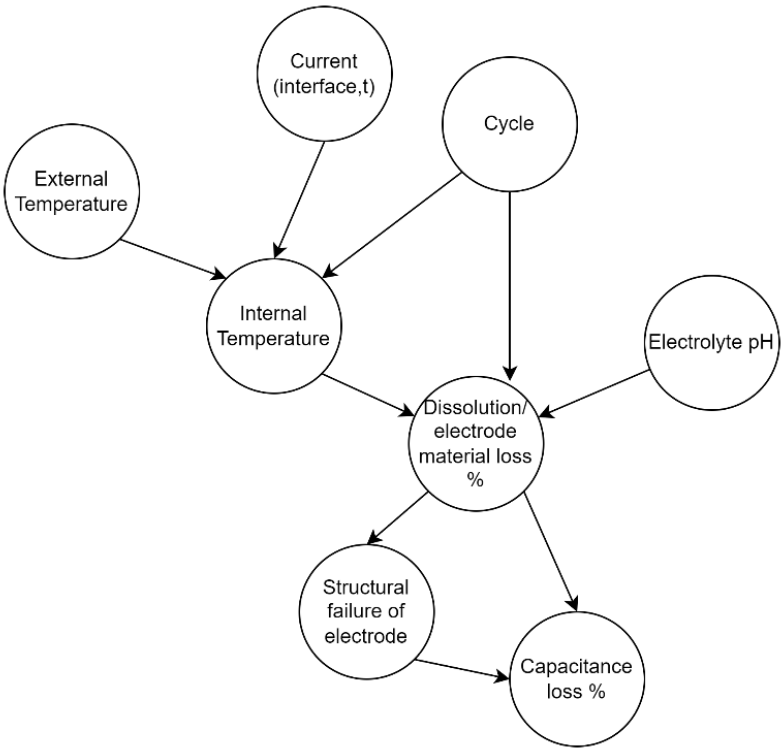

Figure 16. Bayesian Belief Network used for parameter updating, showing the probabilistic relationships used to develop the conditional probability table.

To produce a CPT for the change in internal temperature based on the external temperature, the cycle number, and the current at the interface at a given time, mean values of internal temperature change were pulled from the literature [82, 83, 84, 85, 86]. Data included information such as that shown in Figure 17 where the total increase in temperature after a cycle was used as the mean value. As evident from this data, the internal temperature increases are higher at lower cycle numbers and close to zero at higher cycles. Additionally, the internal temperature increase is higher when the cell experiences higher currents.

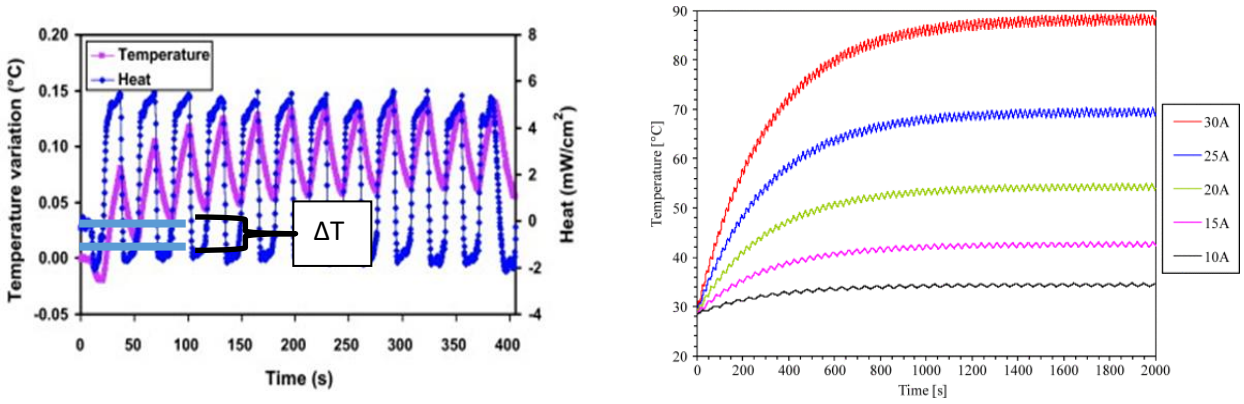

Figure 17. Example of data used to estimate change in internal temperature per cycle. a) highlights an example of a value for ΔT that occurs within the 2nd cycle *[83]*. b) shows the slowing increase in temperature at high cycle numbers and the influence of current *[86]*.

A lognormal distribution was chosen to ensure that the distribution created around these mean values does not include negative values (i.e., decreasing internal temperature). To produce a lognormal distribution, equations (23) and (24) were used to calculate the lognormal mean and standard deviation from the values obtained from literature.

$$\mu = \ln\left(\frac{\mu_X^2}{\sqrt{\mu_X^2+\sigma_X^2}}\right) \tag{23}$$

$$\sigma^2 = \ln\left(1+\frac{\sigma_X^2}{\mu_X^2}\right) \tag{24}$$

The probability distributions from this were then used when sampling the values of variables in the physics-based model. The MATLAB model then selects randomly from discrete intervals of temperature increase based on the probability of being in that interval of temperature increase given by the CPT dependencies on cycle, external temperature, and current. A similar process was followed for estimating the active materials loss in each time step, considering the dependencies on internal temperature, cycle number, and pH [87, 88, 77, 62]. However, a normal distribution is used for this estimation given that there is some probability of increasing active

material from one time step to the next (as suggested by the redeposition process in literature and the increasing capacitance from experimental results). By using this probabilistic information from the CPTs and Monte Carlo sampling of these parameters, the model can propagate uncertainty from the input variables of external temperature and current, for example, to the final output of capacitance. With this propagated uncertainty, sensitivity analysis may also be informative to understand how influential certain inputs are to the final outcome. Figure 18 shows an example concentration profile for the concentrations of the oxidizing agent and reducing agent, c_{ox} and c_{red}, respectively, at each distance (differentiated by colors). Images b and c show the minor changes occurring in each concentration at the 200^{th} cycle as compared to a and b at the 1^{st} cycle.

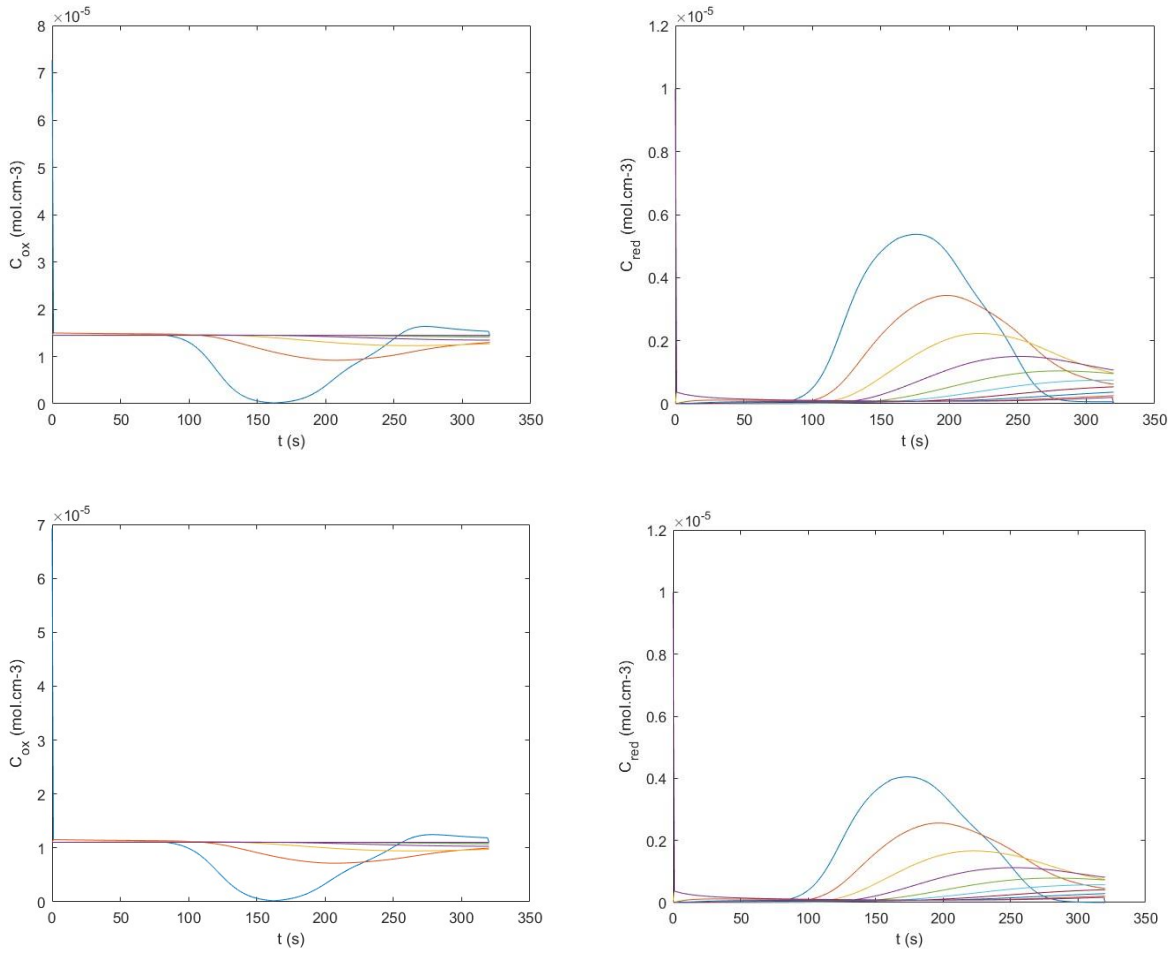

Figure 18. Concentration profiles at the first cycle for a) the oxidant species and b) reductant species. Bottom: Concentration profiles at the 200th cycle for c) oxidant species and b) reductant species.

4.4. Model Results and Validation

The physics-based model of pseudocapacitors developed in this work was calibrated and validated with comparisons between the model's predictions and experimental data, as well as other established models and theoretical predictions. The validation process involved analyzing the model's performance under various scenarios and evaluating its ability to capture various mechanisms evident in cyclic voltammograms. By refining the model iteratively, uncertainties can be reduced, and it can deliver more precise and reliable predictions.

Figure 19 shows the voltage profiles simulated for multiple scan rates, the blue one in this case being the slowest scan rate of 0.005 mV/s. This was the scan rate used for most runs of the simulation. This figure also shows the relative contribution of the faradaic and capacitive currents that are summed in the model for one example case with a slow charge transfer rate. Figure 19, c and d show results of the simulation run at faster (0.01 mV/s) and slower (0.001 mV/s) scan rates, respectively, as compared to the typical value used in this study of 0.005 mV/s.

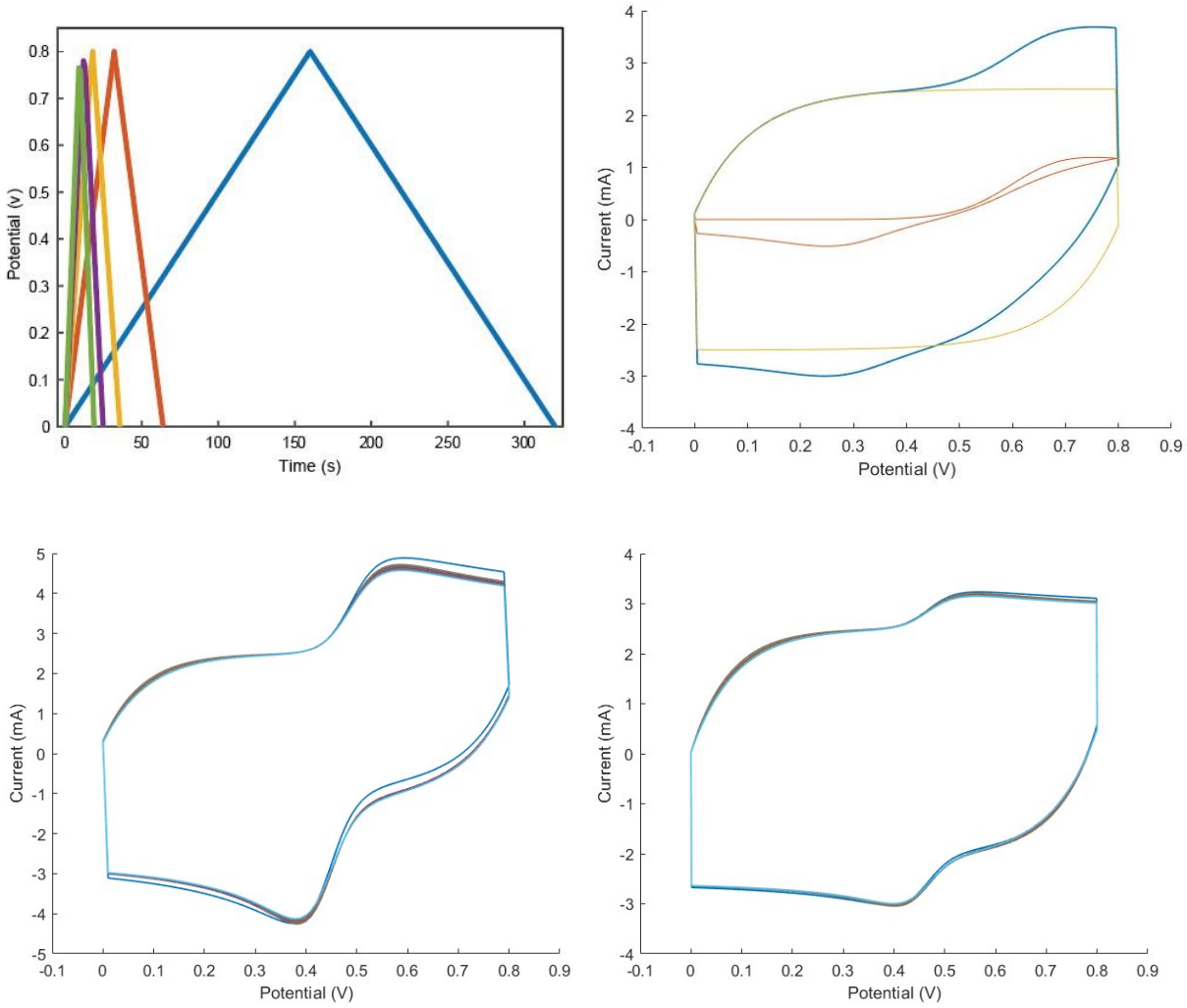

Figure 19. a) Voltage profiles for multiple scan rates from 5mV/s to 100mv/s. (b) Example of simulated CV results with faradaic current in red, capacitive current in yellow, and total current in blue. c) faster scan rate – 0.01 mV/s. d) slower scan rate – 0.001 mV/s.

Figure 20 displays the results of multiple simulation runs, comparing the relative impact of each of these important model parameters. The effect of temperature, with all else held constant, is seen to change the shape of the cyclic voltammogram, with less prominent redox peaks. In the forward scan, for example, it can be thought of as redox reactions beginning to occur at earlier times (lower voltages), as the activation barrier for these reactions becomes lower with temperature. With the combination of other factors, however, such as diffusion coefficients changing with temperature or concentrations changing, this effect may become moderated.

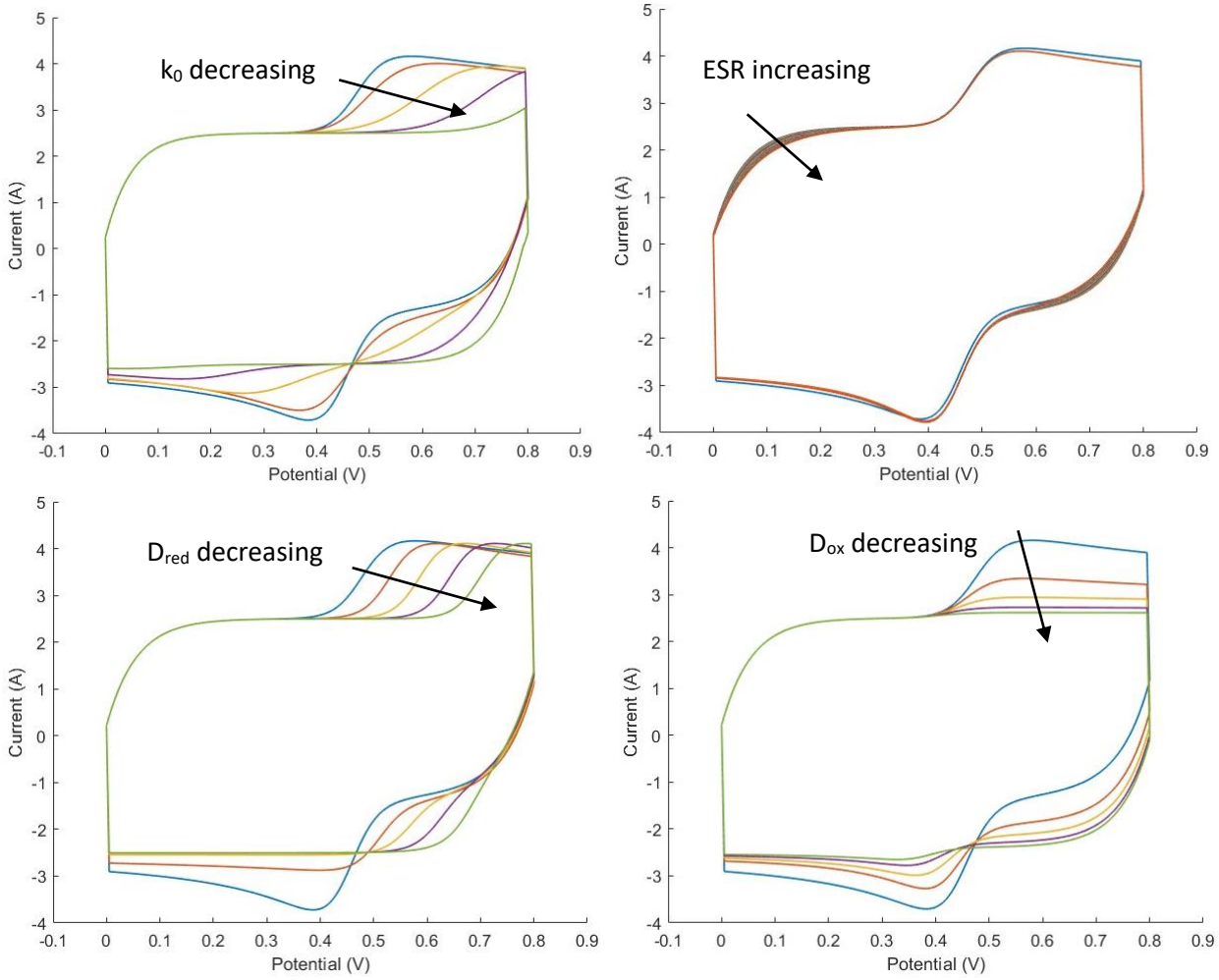

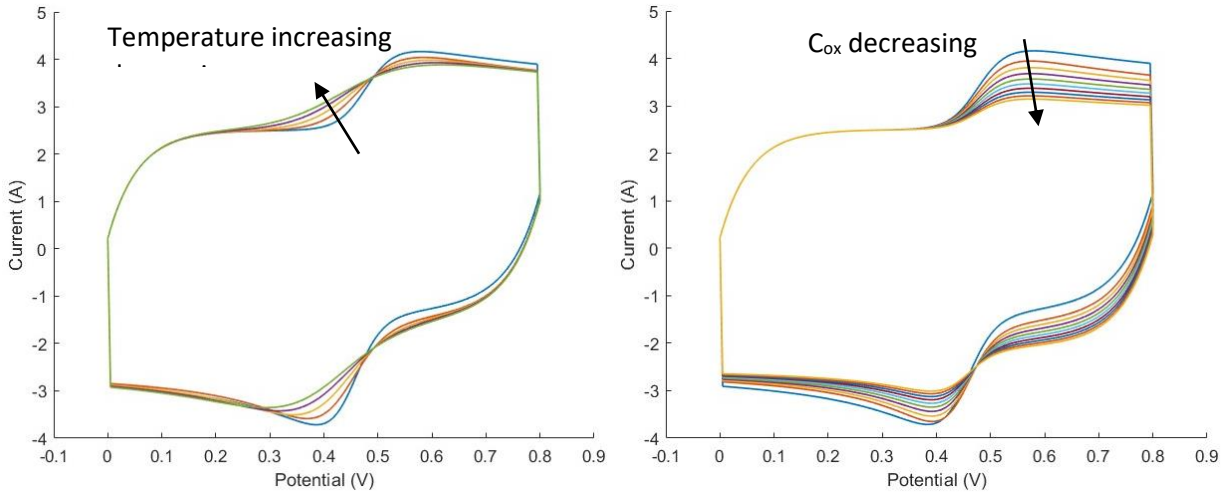

Figure 20. Sensitivity analysis of various model parameters, each simulated while keeping all others constant.

Figure 21 shows results from running the simulation for 500 cycles, including the Bayesian updating for temperatures, concentrations, and resistance values. The CV curves are plotted every 50 cycles. Figure 21b shows the capacitance values over cycling. The model output should also read “failure at X cycles” if the capacitance reaches 80% of the maximum capacitance value. In this case, the simulation did not reach failure at 500 cycles.

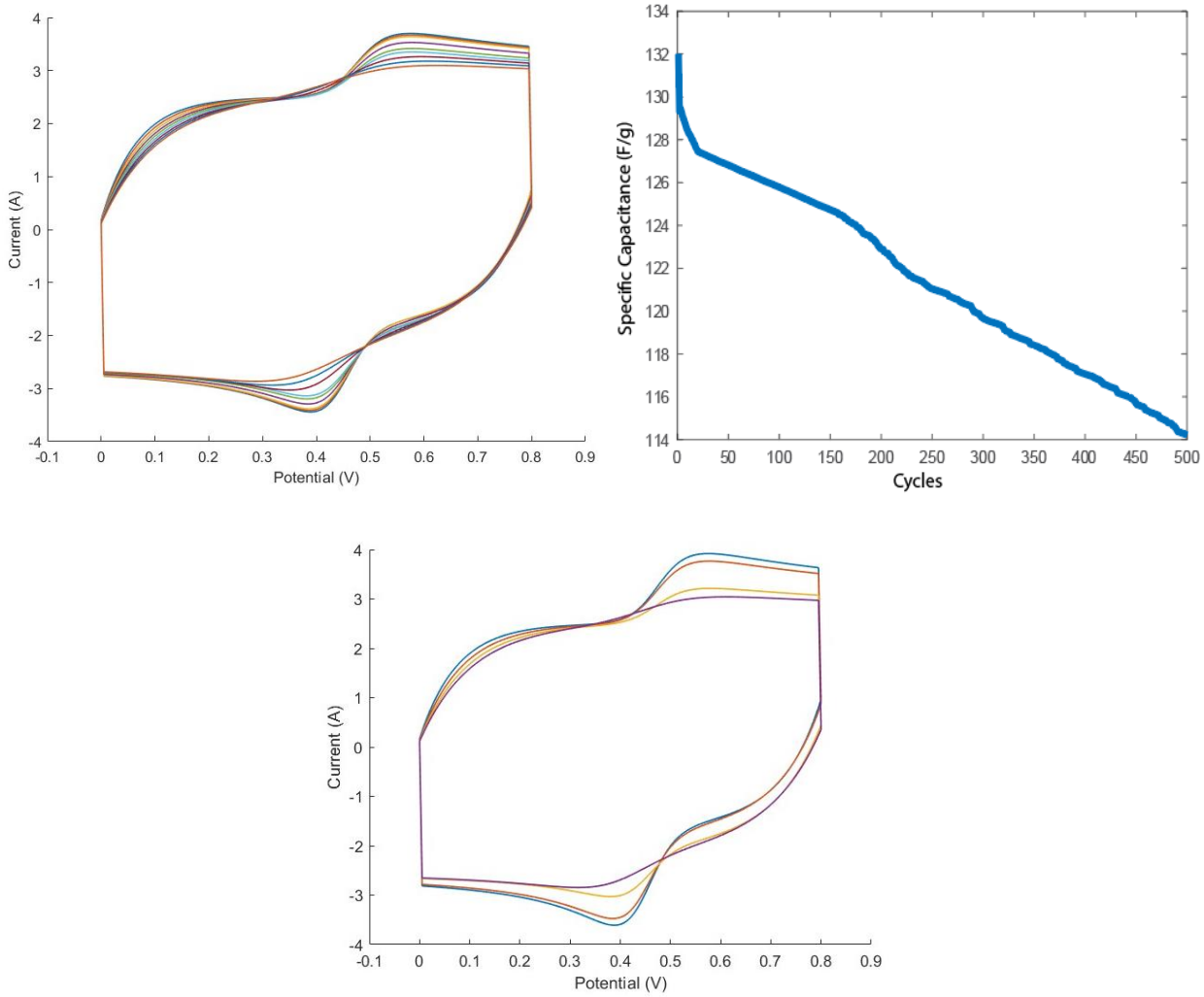

Figure 21. a) 500 cycles (plotted every 50 cycles). b) Specific capacitance over cycles for the run in (a). c) 500 cycles plotted every 100 cycles.

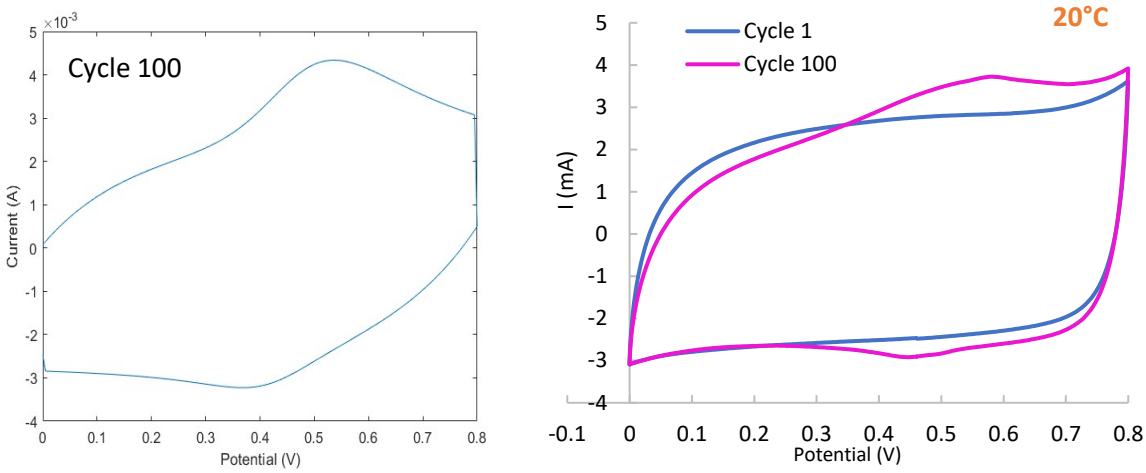

Figure 22. a) cycle 100 of a simulated cyclic voltammogram. b) cycles 1 and 100 of cyclic voltammogram for a real cell collected experimentally.

While the increase in capacitance seen in the real data of Figure 22,b and in Chapter 3 is not captured in every simulation run, the general shape of the cyclic voltammetry curves is replicated by the simulation results, including the locations for the broad cathodic and anodic peaks and the range of values for the specific capacitance over the number of cycles.

4.5. Model Limitations

Some of the main model limitations are:

- The current formulation of the model is in 1D and does not account for volumetric effects such as porosity, which are known to be important factors in the capacitance of devices.
- While the model is highly interpretable, it can be quite complex. The probabilistic methods add robustness and a way to directly model the stochastic processes occurring in the material, but also increase the computational time through numerous sampling steps. Expanding the sensitivity analyses may help with this.

- Assuring proper assignment of probability distributions to the uncertain variables of the BBN is challenging. It requires using expert judgement and deductive reasoning to estimate mean values of the changes that may occur in active material concentration and temperature. This is done by interpolating between known data points, so inaccurate choices may impact the model's predictive capability.
- The model is tuned for MnO_2 devices and may require experimental tests to know certain parameters of the model for other materials. It still, however, is an improvement on the time required to run 10,000 or more cycles on multiple devices to obtain data.

CHAPTER 5

5. Remaining Useful Life Prediction

5.1. Introduction

Remaining useful life (RUL) prediction can take on many forms. Prognostic RUL modes can be statistical and data-driven, physics-based, or a hybrid approach. Hybrid approaches seek to capitalize on the strengths of both data-driven and physics-based models. This can work by integrating a mechanistic understanding of the system into the process of parameter selection for a data-driven model, or conversely, integrating insights from data into a mechanistic understanding of a system.

The MATLAB simulation of pseudocapacitor electrochemistry described in chapters 4 and 5 outputs the capacitance in consecutive cycles, allowing interpretation of the decreasing capacitance, energy, and power density over time. The simulated operation of the pseudocapacitor may change from cycle to cycle, with changes to external and internal temperature, changes to the speed of charge and discharge, changes to voltage requirements, while also predicting the degradation. Therefore, the simulation can more accurately represent specific use cases with different operation schedules, such as a pseudocapacitor as a part of a grid energy storage system, or as part of a regenerative braking system in an electric vehicle. This model is well suited for a combined physics-based and probabilistic method for assisting researchers with exploration of new devices, estimating the lifetime of a pseudocapacitor device subject to real usage scenarios, and optimizing its use in connection with other systems. Accurate RUL predictions from hybrid models with enhanced reliability will be especially important for critical systems, such as energy infrastructure, where failures can have significant consequences.

For electrochemical energy storage technologies like batteries or supercapacitors, a device is generally accepted to have reached end of life when it reaches 80% of nominal capacity. For this study, this threshold is also considered failure for pseudocapacitors. While some have conducted cycling and stability studies of pseudocapacitors [15], no researchers have attempted to predict the expected RUL for these devices. As with most other systems, RUL predictions are likely to change depending on the environmental and operating conditions. For planning and operating systems optimally, it is useful to know what one might expect from an energy storage device that has previously experienced specific conditions. While these predictions have been made extensively for batteries and are increasingly being analyzed for supercapacitors, the charge transfer kinetics of pseudocapacitors are unique, highly susceptible to environmental and operating conditions, and require their own RUL predictions.

5.2. Probabilistic lifetime model

Probabilistic models utilize knowledge about a system or system components which can be defined using a probability density function (PDF). This function describes the likelihood of a random variable falling within a particular range of values rather than one deterministic value. Common model choices include, exponential, Weibull, and lognormal distributions, among many others. The parameters of the distribution are estimated from data and the chosen distribution can then be used to describe the probability distribution of failure times. Given the historical data and the fitted model, the RUL can be estimated. As new data becomes available, the model can be updated to improve the accuracy of RUL predictions.

Uncertainty propagation is a feature of RUL and other probabilistic analyses that helps enhance decision-makers' understanding of how variations in input parameters impact failure and risk outcomes. Uncertainty propagation is often used to assess risk outcomes by considering the

uncertainty in input data parameters. This is particularly useful when there are complex correlations between parameters, as previously discussed in this chapter. These methods aid decision-makers in expressing their assessments as a probability of a certain outcome with a defined confidence interval. One approach to uncertainty propagation is Monte Carlo Simulation. Monte Carlo Simulation generates random numbers to sample from a distribution of each input variable, calculates the outputs and can then display the level of certainty one has of obtaining those outputs based on the uncertainty of input parameters.

To propagate the parameter uncertainty to the RUL output of the degradation model in this simulation, a Markov Chain Monte Carlo (MCMC) method was used. In this process, many samples of the parameters are generated from the posterior distribution and the degradation model in equation (25). The Monte Carlo method is Markovian because the values are sampled consecutively, and the future state only depends on the current state. As more samples are generated, the samples more closely approximate the posterior PDF. A uniform proposal function is used as a part of the MCMC sampling process. This function generates candidate parameter values for each next iteration of the MCMC simulation. When the Markov chain reaches a stationary distribution, the samples can be considered representative of the target posterior distribution. An illustration of this process is shown in Figure 23.

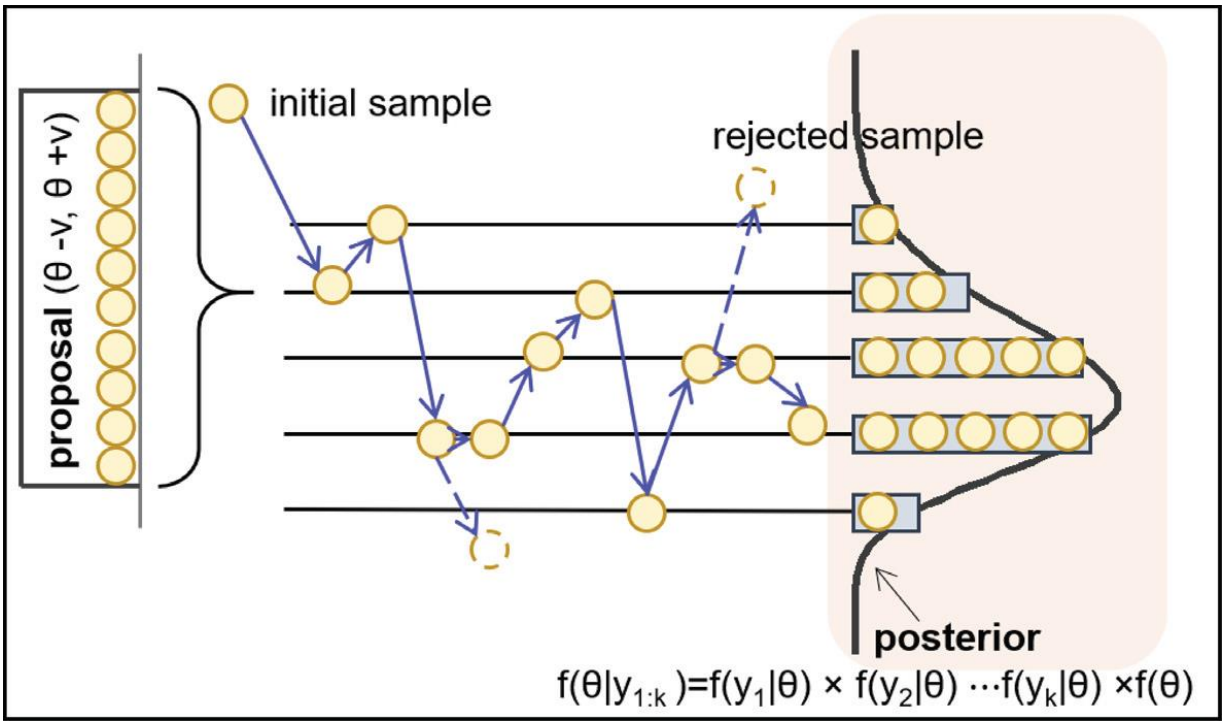

Figure 23. Illustration of Markov Chain Monte Carlo process, with sampling from proposal distribution, and uncertainty propagated to posterior distribution in the form of a histogram *[89]*.

In this research, pseudocapacitor RUL was estimated using a Bayesian prognostics model. The model takes inputs for any number of cycles of known capacitance values and predicts the length of time (or number of cycles) the device can operate (assuming fully charging and discharging) before it goes below the threshold value of 70-80% of the initial specific capacitance. A degradation model of the exponential form$y=a\cdot exp(-bt)$ (25) was used, as this has been shown to be applicable to the degradation of capacitance or increase in resistance as a function of time or cycles in various studies of battery lifetime prediction [89, 90, 91].

$$y = a \cdot exp(-bt) \tag{25}$$

More details on model selection can be found in section 5.3.

In this equation, *y* can represent internal battery or supercapacitor parameters such as capacitance or resistance which are measurable indicators of degradation. When fit to data, b = 0.001. This was tested against the real data in Figure 24 at 50°C, using the first 10 values after the peak in capacitance as the initial data for the RUL model. The capacity retention for this cell was just 82% at 200 cycles, close to the failure threshold of 80%. Given the initial data, and setting the threshold to 82% of initial capacity, the model predicts approximately 102 cycles after these initial 35 cycles (75 cycles at the 5^{th} percentile, and 198 cycles at the 95^{th} percentile). Compared to the real value of approximately 165 cycles to failure, the model slightly underestimates the RUL of the cell. The real value, however, is within the bounds of the model's uncertainty. A similar prediction for a cell tested at 40°C was made, with median of 8 cycles of remaining useful life after the peak (5 cycles at the 5^{th} percentile and 12 cycles at the 95^{th} percentile). The real data shows failure approximately 37 cycles after the peak, which is outside the confidence intervals of the RUL prediction. This suggests that the RUL prediction cannot be generalized for varying environmental conditions when the parameters are chosen based on limited data.

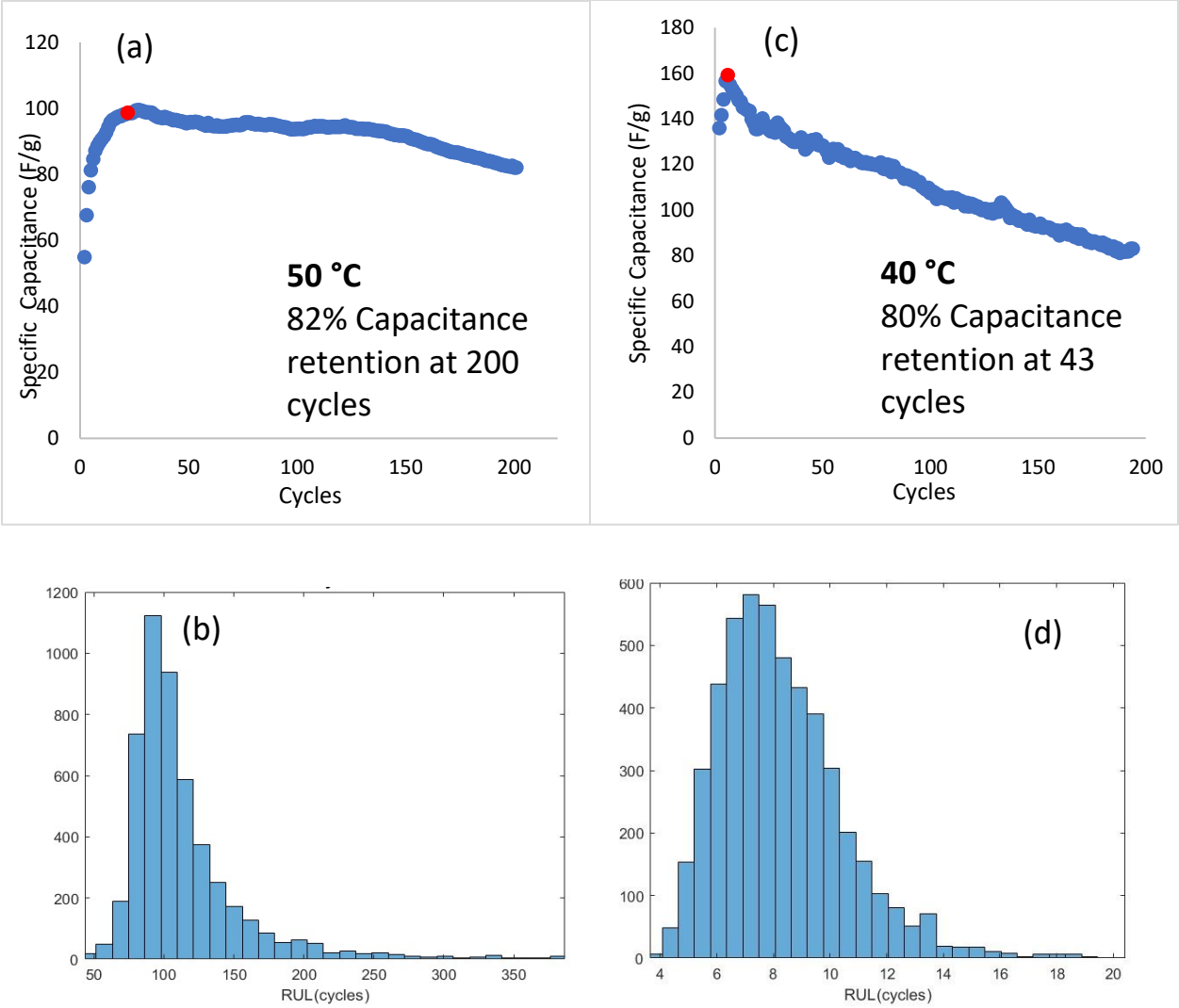

Figure 24. a) Specific capacitance changes with cycles at 50C. b) Histogram of RUL for 50C. c) Specific capacitance changes with cycles at 40C. d) Histogram of RUL for 40C.

For cells operating under differing environmental conditions, the parameters *a* and *b* may need to be chosen with more precision. For EDLCs, some researchers have represented capacity attenuation with an Arrhenius equation of the form,

$$C_{loss} = A \cdot \exp\left(-\frac{E_a}{RT}\right) \cdot N^z$$

Where A is a pre-exponential parameter, N is the cycle number, and z is the power index parameter [53]. The activation energy E_a was also examined to be a linear function of the electric

current. With this formulation, the model can more explicitly capture the impacts of temperature and current. However, this was only applicable within the temperature range of 25-55 °C and is limited to these inputs as parameters of the model.

In the present study, parameters *a* and *b* were also then fitted to data that detail the specific capacitance values of MnO_2 pseudocapacitors over numerous cycles under different conditions of temperature, scan rate. Cycle life data with different electrolyte pH were also collected. With theoretical cycle stability on the order of 10,000 or more cycles, running multiple long term cycling tests for that length of time proved intractable. Therefore, experimental data collected was supplemented with many data points pulled from existing literature on the same or similar MnO_2 pseudocapacitive devices. The shorter experimental tests conducted in this research obtained capacitance values in the first 200-300 cycles of operation. These tests were valuable to train the model for early stages of cycling, wherein experimental observations and literature show large variations in capacitance (e.g., sharply increasing, sharply decreasing, or oscillating). With these data of capacitance over cycles for different combinations of temperature and scan rate, curve fitting was done in a MATLAB application using a nonlinear least squares method. With this methodology, other environmental and operating conditions (beyond temperature and scan rate or current) that may impact the lifetime of the cell may be more readily incorporated into the degradation model through the selection of parameters to be used in equation (25).

Isolating temperature as a factor impacting the parameters, the scatter charts in Figure 25, were obtained. These feature parameters fit to data collected from experiments in this study and experiments throughout the literature. Except for parameter b in the power law case, there seems to be very little correlation between the parameters and the outputs, suggesting that the power

law may be the best suited fit for representing the degradation in capacitance, or more likely, that more data is needed to assess the impact of temperature on parameters.

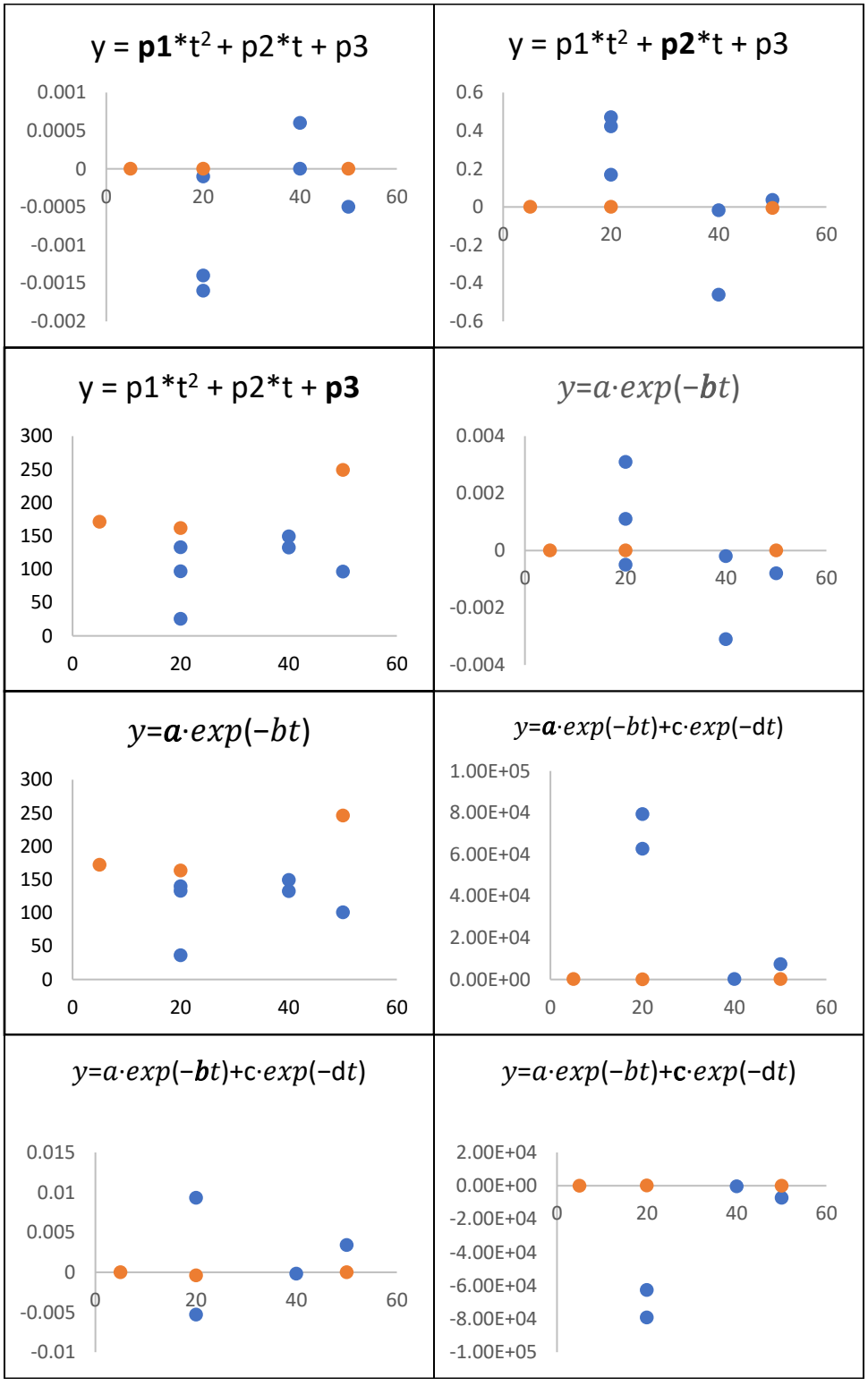

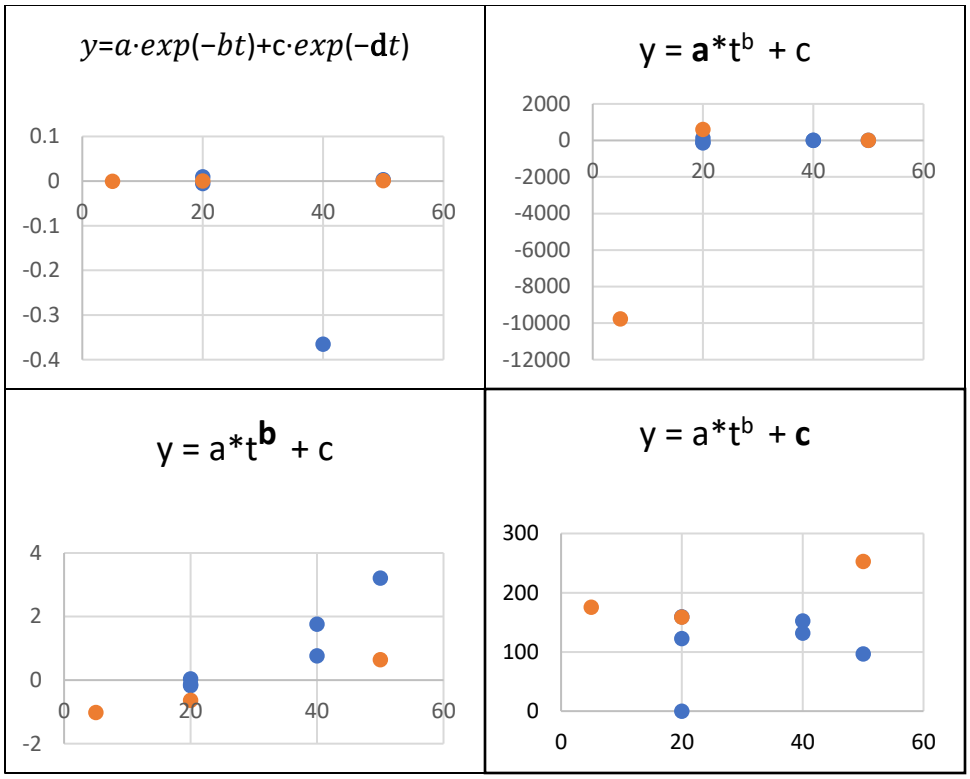

Figure 25. Correlations between parameters and changing temperature (x axis) for a polynomial model, an exponential model, a two-term exponential model, and a power law model. (Bolded letters within equations are the parameters represented on the y axis for that given model).

To assess the correlation of variables, they were also assessed simultaneously. The values of a and b for the different combinations of temperature and scan rate are shown in Table 2.

Table 2. Table of hyperparameters fit to data for the exponential model.

Temperature (°C)	Scan Rate (mV/s)	a	-b
20	1		
20	5	139.7206	-0.0005
20	5	133.2232	0.0011
20	5	36.225	0.0031
20	5	41.7252	-1.00E-20
20	5	296.9563	-1.00E-20
20	10		
20	20	694.3342	-0.0001
20	100	259.1189	-1.00E-20
20	100	179.9263	-0.0004

20	100	58.3902	-1.00E-20
20	100	163.7287	-1.00E-20
20	200	237.7389	-0.0001
20	5	139.7206	-0.0005
20	5	133.2232	0.0011
20	5	36.225	0.0031
40	5	149.2615	-0.0031
40	5	132.5438	-0.0002
50	5	100.8964	-0.0008
5	100	172.3421	1.00E-20
20	100	163.7287	-1.00E-20
50	100	246.1486	-1.00E-20

When selected to represent the conditions of the system in the RUL model, the parameters *a* and *b* can be considered functions of temperature and scan rate. Instead of semi-arbitrarily choosing parameters for the RUL model, this allows for the model to become more representative of real conditions and continually improve with more data. Multiple linear regression of the two independent variables, temperature (T) and scan rate (υ), were calculated with degradation model hyperparameters *a* and *b* representing the dependent variables. The multiple linear regression equation took the form:

$$a = \propto T + \beta\upsilon + \varepsilon \tag{26}$$

Where α and β are the coefficients associated with each independent variable, with an error term ε. A least squares regression was computed in MATLAB. With this regression, we can choose the best mean values for *a* and *b* in the exponential degradation model based on the best-fit surface for a desired temperature and scan rate. Results of the best-fit surfaces for *a* and *b* are shown in Figure 26.

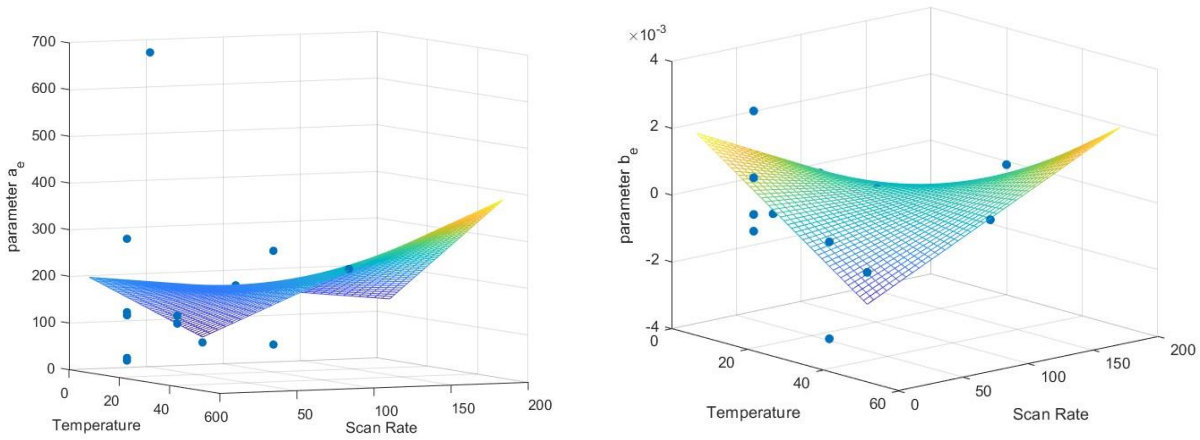

Figure 26. Best fit surfaces for parameters a and b of exponential model.

The data is sparse, the RMSE is quite high, and the R^2 value is only approximately 0.04 for parameter *a* and 0.29 for parameter *b*. With the current data of temperature and scan rate together, we do not seem to get much more information about the hyperparameters *a* and *b* than we did knowing each individually. Another input, such as voltage together with temperature, might contribute more information about the parameters. However, the RUL model can still run with these preliminary estimates of the model parameters for different temperatures and scan rates and continuously improve the prediction with new datasets. Further, in the Bayesian prognostics used to predict RUL, these values represent initial beliefs about the parameters *a* and *b*, which will be updated with a likelihood function to obtain a posterior probability of these parameters given the capacitance data input to the prognostics algorithm. The fitted regression equations for *a* and *b* are shown below.

$$a = 214.3597 - 2.1767T - 0.5576v + 0.0388 \cdot Tv$$

$$b = 0.0025 - 0.000087T - 0.000024v + 0.000000859 \cdot Tv$$

Using common values from experimental conditions, T=20C and υ=5mV/s, these regression equations return a = 171.913 and b = 722.9E-6 for a room temperature degradation model

$$y = 171.913 \cdot exp(-722.9 \times 10^{-6} \cdot t)$$

A uniform prior distribution $f(parameters) = f(a) \cdot f(b)$ (27) was chosen, representing initial beliefs about the parameters a and b of this degradation model. A likelihood function for a given capacitance data point (input to the model) was then obtained (equation 28) representing the probability of observing the available data given the possible values of the model parameters. The likelihood for multiple data points is given by the product of their likelihoods. Bayes theorem (equation 29) was then applied to update the prior distribution based on the observed data.

$$f(parameters) = f(a) \cdot f(b) \quad (27)$$

Where $f(a) \sim U(a_{min}, a_{max})$ and $f(b) \sim U(b_{min}, b_{max})$

$$L(data|parameters) = \frac{1}{\sqrt{2\pi}} \cdot \exp\left(-\frac{1}{2}\left(data_{i_m} - data_{i_c}\right)^2\right) \quad (28)$$

Where $data_{i_m}$ represents measured data and $data_{i_c}$ represents calculated data.

$$f(parameters|data) = \frac{L(data|parameters) \cdot f(parameters)}{f(data)} \quad (29)$$

$f(data)$ can be considered as a normalizing constant. Finally, the form of the distribution for N data points is

$$f(parameters|data) = \frac{1}{K\sqrt{2\pi}} \cdot \exp\left(-\frac{1}{2}\sum_{i=1}^{i=N}\left(data_{i_m} - data_{i_c}\right)^2\right) \cdot f(parameters) \quad (30)$$

The updated distribution, the posterior distribution, represents the updated beliefs about the RUL given both the prior information and the likelihood. Because the prior knowledge is represented

as distributions, the posterior is capable of characterizing the uncertainty in RUL estimation propagated from the uncertainty of the underlying data.

5.3. Model Determination for RUL Prediction

While previous research suggested the exponential degradation model used above for degradation of batteries or EDLCs, the data obtained in the present research variably fit well to other models. The exponential model especially seems unfit for early cycle capacitance data that is increasing due to activation processes discussed in Chapter 3. Figure 27 shows erroneous RUL predictions for a sample tested at room temperature, which displayed increasing capacitance over 100 cycles, unlike those at elevated temperatures that reach a maximum capacitance value within 30 cycles (after which RUL predictions were made). Median RUL prediction after the first 10 cycles was 83 cycles, with 60 cycles at the 5^{th} percentile and 92 cycles at the 95^{th} percentile. Given the real data showing continuously increasing capacitance beyond these values, the model does not seem capable of predicting RUL for cells that experience an extended activation process.

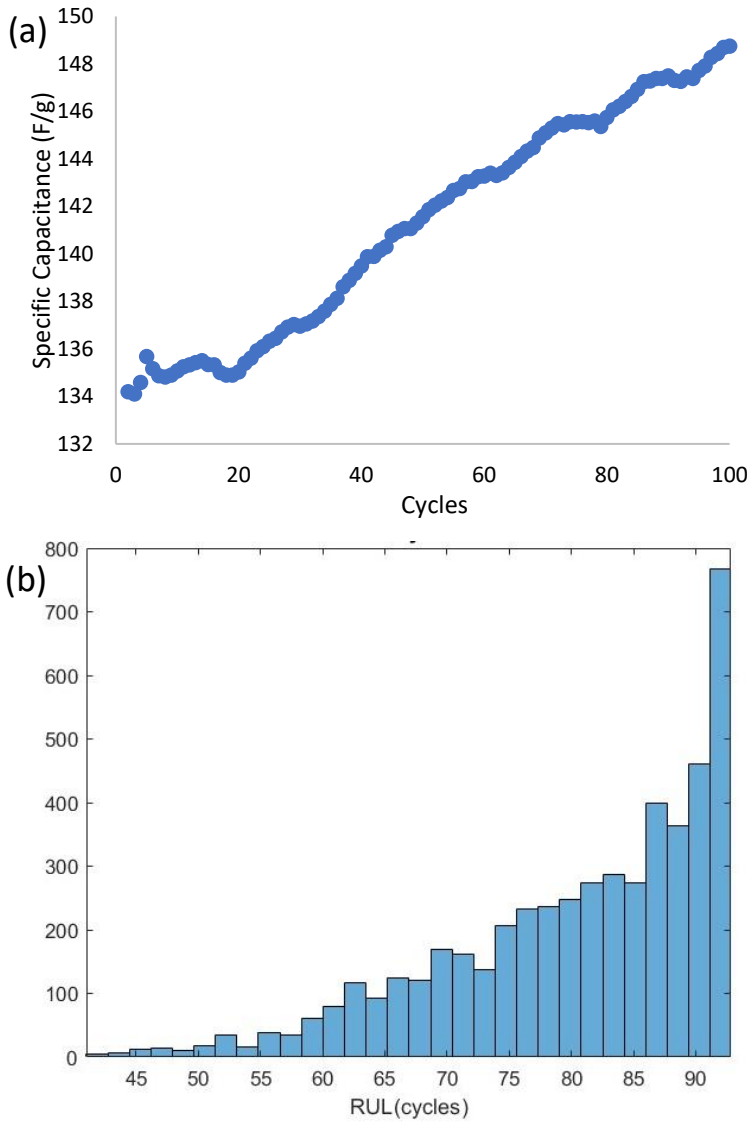

Figure 27. a) Specific capacitance over 100 cycles at room temperature. b) Histogram of predicted RUL

With this behavior, other models like a two-term exponential function or a power law model (equations (31) and (32), respectively) may be better suited as degradation functions to predict the remaining useful life.

$$y = a \cdot exp(-bt) + c \cdot exp(-dt) \tag{31}$$

$$y = a \cdot t^b + c \tag{32}$$

Following the same method as with the exponential model, a power law model and a two-term exponential function were also fit to the data to ensure selection of the best model. Table 3 and Table 4 show the values of the hyperparameters at the same temperature and scan rate combinations for the two-term exponential function and power law, respectively.

Table 3. Table of hyperparameters fit to data for the two-term exponential model.

Temperature (°C)	Scan Rate (mV/s)	a	b	c	d
20	5	7.93E+04	-0.0053	-7.92E+04	-0.0053
20	5	6.27E+04	0.0093	-6.27E+04	0.0093
20	5	62740	0.0093	-62707	0.0093
20	5	9.3082	-0.0014	37.1021	1.00E-20
20	5	11.8923	-0.0087	291.8292	-1.00E-20
20	20	39.3361	-0.0376	680.5523	-1.00E-20
20	100	260.3959	-1.00E-20	-46.2256	-0.0018
20	100	30.4596	-0.015	156.9199	-1.00E-10
20	100	4.24E+04	-7.06E-05	-4.23E+04	-7.07E-05
20	100	9.0735	-0.0004	159.246	-1.00E-20
20	200	15.0403	-0.0217	229.9379	-0.0001
20	5	-0.0009	0.075	132.9113	0.0012
20	5	-1.49E+06	0.01	1.49E+06	0.01
20	5	-1492300	0.01	1492400	0.01
40	5	3.3917	-0.0768	148.2568	-0.0031
40	5	132.7178	-0.0002	-38.9375	-0.2352
50	5	3.88E+06	0.0041	-3.88E+06	0.0041
5	100	172.136	1.00E-20	-105.8954	-0.0044
20	100	163.7543	-1.00E-20	-18.302	-4.80E-03
50	100	245.4988	-1.00E-20	-39.9046	-0.0134

Table 4. Table of hyperparameters fit to data for the power law model.

Temperature (°C)	Scan Rate (mV/s)	a	b	c
20	5	-80.7115	-0.1758	159.4606
20	5	123.7011	0.0361	0
20	5	-129.4363	-0.1354	122.5819
20	5	14.1605	-0.3593	40.4227
20	5	-164.4793	0.0151	472.621
20	20	55.936	-0.3641	671.6245
20	100	-107.3574	-0.2118	273.9984
20	100	-9.7282	0.2497	197.652
20	100	91.1585	-0.0697	0
20	100	596.2894	-0.6351	158.4313
20	200	-10.0511	0.1964	256.4337
20	5	-80.7115	-0.1758	159.4606
20	5	123.7011	0.0361	0
20	5	-129.4363	-0.1354	122.5819
40	5	-1.2634	0.7676	152.4603
40	5	-0.0003	1.7557	131.5632
50	5	-1.00E-20	3.2063	96.6481
5	100	-9770.7	-1.0236	175.6667
20	100	596.2894	-0.6351	158.4313
50	100	-0.0972	0.6436	252.7685

With the available data, the best fit surfaces to correlate these operating conditions with the parameter values for the power law model are shown in Figure 28.

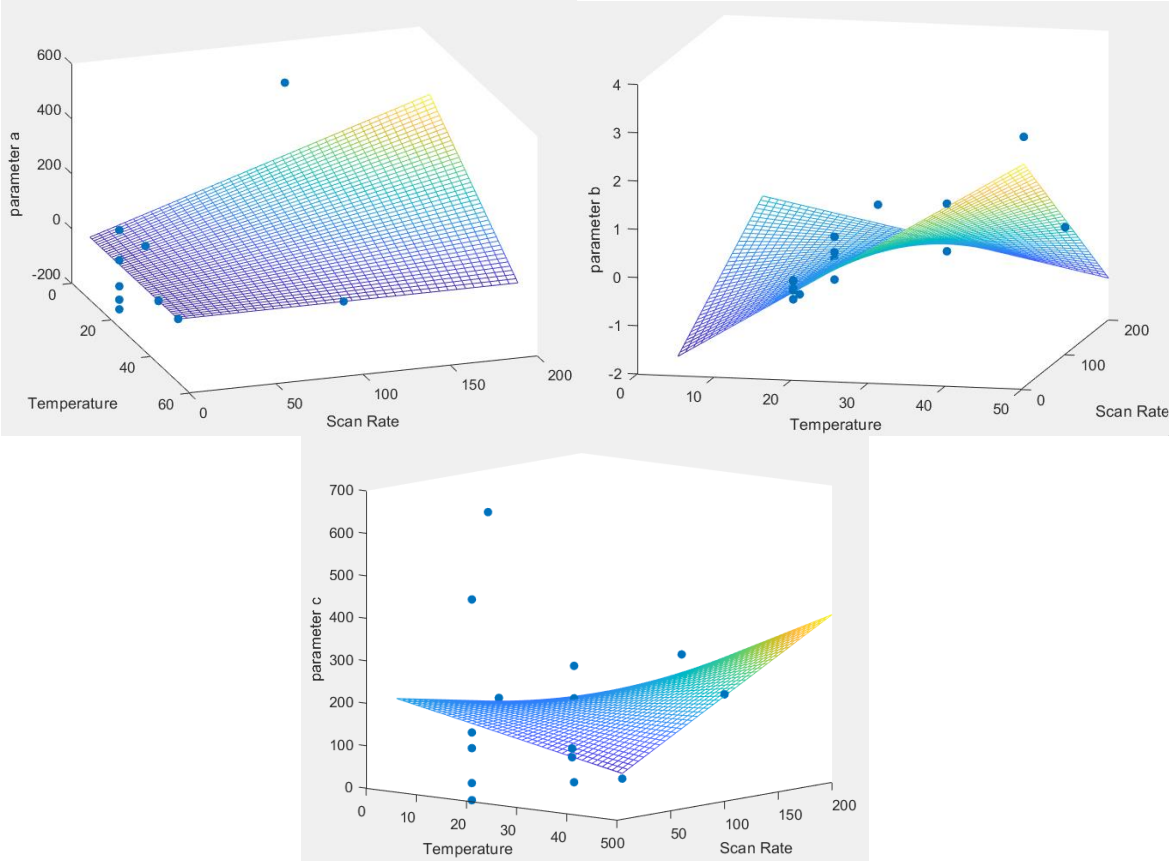

Figure 28. Best fit surfaces for parameters a, b, and c in the power law model

While there is not great correlation value for the parameters a and c (R^2 = 0.13 and R^2 = 0.03 respectively), parameter b has a relatively high R^2 value of 0.86 and a best fit surface showing some correlation with changes in operating parameters. The equations to obtain parameters for the power law model based on the temperature and scan rate are shown below.

$$a = -13.1135 + 0.25939T + 2.2105\upsilon - 0.0442 \cdot T\upsilon$$

$$b = -2.1812 + 0.09832T + 0.01309\upsilon - 0.000648 \cdot T\upsilon$$

$$c = 232.2172 - 2.6137T - 0.73492\upsilon + 0.04415 \cdot T\upsilon$$

When used in the Bayesian Monte Carlo method for RUL, the model does not converge to a RUL value, suggesting adjustments to the Monte Carlo method are required. Additionally, more data is needed to better refine parameters.

5.4. Integration with Physics-based Lifetime Model

5.4.2. Model Weighting Based on Uncertainty

Physics-based models (as described in chapter 4) involve simulation of a system based on the underlying physics and engineering principles, requiring a deeper understanding of the physical processes and mechanisms that govern operation, degradation, and failure. The parameters of these models represent material properties and environmental conditions which are calibrated and validated from experimental data or literature. This approach is beneficial for its interpretability and generalization to varying conditions but is inefficient for capturing all uncertainties and random variations. A hybrid approach, combining the physics-based model with a probabilistic model, allows for accounting of uncertainties and variations that are not explicitly captured by the physics-based model. This is done directly in the pseudocapacitor physics-based model with Monte Carlo sampling of parameters (e.g., resistance, concentration, temperature), which are empirically adjusted from one time or cycle step to the next based on observed data. Further the combination of predictions generated by both models can lead to more robust and accurate predictions and further support decision making. This combination can be done by weighting the predictions from each model based on the confidence or uncertainty of each of their outputs. This ensemble approach, as done by [92], represents the weight as the standard deviation at a point in the model in ratio with the maximum standard deviation for the model's prediction.

$$\lambda_i = \frac{\sigma_i}{\sigma_m}$$

Capacitance value outputs of the probabilistic and the physics-based model are integrated into a single output based on the weighting of each model's uncertainty, as shown in equation (33).

$$y_h = (1 - \lambda) y_{m1} + \lambda y_{m2} \tag{33}$$

This method is useful in cases such as this one, where the physics is only partially known or represented, and the data is limited. Information from the data and the physics and their known uncertainty can reduce overall uncertainty and improve the prediction accuracy. Further, another weighting factor can be added by the user to express their degree of confidence in either model based on their knowledge of the given system.

5.4.3. Bayesian Model Uncertainty

With multiple models of reasonable accuracy, another method of integrating models utilizes Bayesian model averaging. Bayesian model averaging can ostensibly provide better predictive performance, especially when one has multiple partially applicable models [93]. With Bayesian model averaging, the various models can be averaged for an optimal prediction y_h with the distribution

$$p(y_h|D) = \sum_{i=1}^{N} p(y_h|M_i) p(M_i|D)$$

Where $p(M_i|D)$ is the posterior probability of model M_i, with data D.

$$p(M_i|D) = \frac{p(\mathrm{D}|M_i) p(M_i)}{\sum_{i=1}^{N} p(\mathrm{D}|M_i) p(M_i)}$$

This method, however, assumes that the models assessed are collectively exhaustive of all possible models. To characterize the uncertainty of predictions based on what is known about the

models of their outputs, we can use a Bayesian model uncertainty. We can assess the uncertainty around model predictions by developing the probability distribution π(y), the distribution around the unknown true value of y_h, or more simply the distribution of y given all available evidence that may be relevant (i.e. D—the known information about the model, and y^*—the model prediction). Using Bayes theorem, the posterior distribution of the output y (e.g. the value of capacitance/remaining useful life) is

$$\pi(y|y^*, D) = \frac{L(y^*|D, y)\pi_0(x)}{\int_x L(y^*|D, y)\pi_0(x)}$$

$$L(y^*|D, y) = L(y^*|D\ \ , y)L(D\ \ |y)$$

Where π_0 is the prior distribution and $L(y^*|D, y)$ is the likelihood function [94].

When using the outputs of the electrochemical model and the RUL model to predict future behavior of a device, one can use a credibility factor, φ, as a weight for the likelihood equation of each model under a given context or ψ as an applicability factor under a different context. This factor are between 0 and 1 for lowest and highest confidence, respectively, and may be based on the analysts confidence that the model will properly predict y under these contexts. The likelihood function gets modified as [94]

$$L(y^*|D, y) = \iint_{\varphi\ \psi} [L(y^*|D_M, y)]^{\varphi\psi}\pi(\varphi|I_c)\pi \cdot (\psi|I_a)\, d\varphi d\psi$$

Where I_a and I_c are information on applicability and credibility, respectively.

With multiple models that may be dependent on each other, coupling them by averaging may just multiply the amount of error. To deal with this dependence the likelihood function can be

constructed as a joint probability distribution of the likelihoods from both models $L(y_1, y_2|y)$ expressed as marginal distributions through a copula function.

5.5. Discussion

The present study aimed to predict the RUL of pseudocapacitors under varying operating conditions. While the RUL prediction showed promise in some situations, the model's performance becomes compromised when confronted with changing environmental factors, such as temperature. As seen in the results, deviations between predicted and actual RUL values became more pronounced in scenarios involving significant temperature variations. This finding raises important considerations regarding the generalizability and robustness of the model in real-world applications where dynamic environmental conditions are common. Several factors may contribute to the observed discrepancies. Firstly, the training dataset might not have adequately represented the full spectrum of temperature conditions encountered during the operational life of the system and may also need to include other types of variation such as electrolyte degradation, variations in deposition processes or voltage dependencies. The model and parameters may not have explicitly accounted for the influence of temperature or other factors on the degradation processes, especially in early cycle life when activation processes are occurring in the material prior to degradation. In practical applications, especially in use cases where temperature variations are inherent, the limitations identified highlight the importance of developing adaptive RUL prediction models. Consideration should be given to implementing real-time monitoring systems that continuously update the model parameters based on the current environmental conditions, ensuring a more accurate and responsive RUL prediction. Overall, this model contributes to the body of work that addresses the challenges of temperature-dependent RUL prediction and provides a foundation for future research aimed at addressing these

challenges and improving the reliability of prognostic models in dynamic operational environments.

CHAPTER 6

6. Case Studies and Applications

6.1. Case Study

EDLCs, with their distinct electrochemical properties, have garnered attention for use in regenerative braking systems, which aim to recover and store kinetic energy during vehicle deceleration. The utilization of energy storage systems regenerative braking is integral to enhancing overall fuel efficiency and reducing energy consumption. Batteries, commonly employed in hybrid and electric vehicles, face challenges with the high power charging during regenerative braking, leading to degradation and performance issues. As mentioned in Chapter 1, supercapacitors and pseudocapacitors offer notable advantages, such as high power density and potentially excellent cycling properties. making them particularly well-suited for the rapid charge and discharge cycles inherent in regenerative braking. While the predominant focus has been on batteries and supercapacitors, this chapter presents a case study for the potential incorporation of pseudocapacitors into regenerative braking systems. Despite the increasing adoption of electric vehicles, the specific exploration of pseudocapacitors in regenerative braking systems remains an underexplored area. This gap in research prompts a closer examination of the electrochemical characteristics of pseudocapacitors for optimal operation, positioning, and sizing within the context of regenerative braking. The distinct charge storage mechanism of pseudocapacitors, combining features of both capacitors and batteries, positions them as a compelling candidate for efficiently capturing and releasing energy during braking events. Further, the fast usage of the stored charge during regenerative braking may circumvent issues arising due to the self-discharge characteristics of pseudocapacitors, which could lead to lower overall system reliability in various other stand-by operations (e.g., grid operations). Because energy stored

during braking will likely be used within seconds to minutes after charging, the energy losses due to self-discharge are likely to be relatively small. Overall, the use of pseudocapacitors in regenerative braking has implications for addressing the limitations associated with traditional battery technologies and improving the overall performance and longevity of energy storage systems in electric vehicles. The models presented in this dissertation can be utilized to optimize electric vehicle systems. Optimized systems including pseudocapacitors have the potential for longer driving range and extended battery lifetimes.

To simulate a hybrid pseudocapacitor braking system, a simplified model of an electric vehicle under standard conditions was created. the sample driving schedule used by the United States Environmental Protection Agency (EPA) for vehicle fuel and emissions testing was used as an input [95]. This is shown in Figure 29.

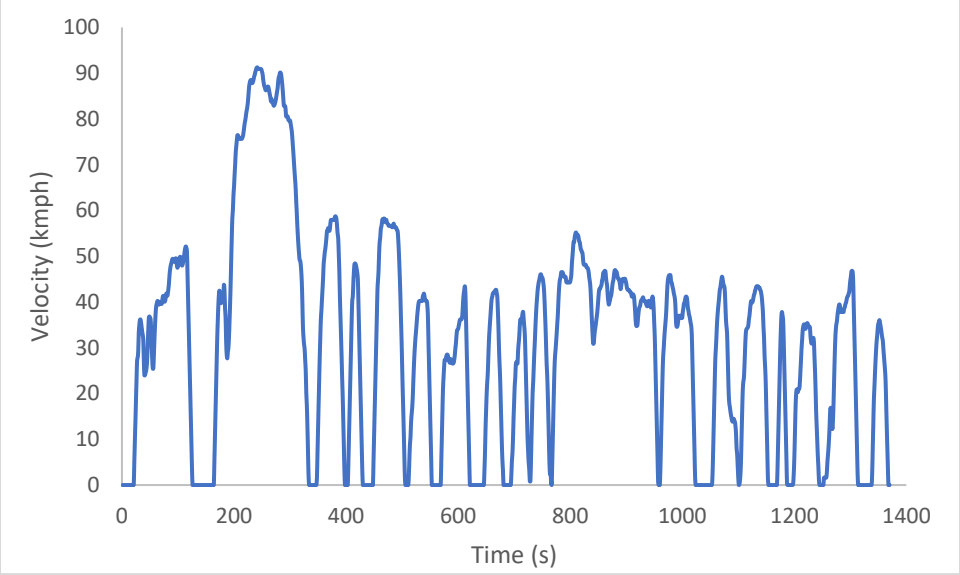

Figure 29. EPA Urban Dynamometer Driving Schedule

Other inputs are the assumed vehicle mass, and other forces on the vehicle. The behavior of the vehicle can be described by

$$F_{TotalTraction} = F_a + F_r + F_g + F_d$$

$$P = F_{TotalTraction} \cdot Velocity$$

The simulation recharges the pseudocapacitor pack at, for example, 300 A during each of the declining velocity (braking) portions of the driving schedule in Figure 29. This exercise is left for future research.

CHAPTER 7

7. Summary

This dissertation aims to identify the degradation mechanisms affecting the performance and reliability of MnO_2 pseudocapacitors under varying operating conditions. Through experimental studies, modeling, and probabilistic analyses, the research focuses on elucidating the dissolution of the electrode material into the electrolyte, as it relates to capacitance reduction. Factors such as voltage sweep rates, temperature, pH, and cycling were studied to identify key contributors to degradation. The objective is to enhance the feasibility of pseudocapacitors for sustainable energy storage systems and enhance the longevity of systems that incorporate these devices.

A physics-based model was developed to simulate the capacitance and degradation behaviors of pseudocapacitors over time. This model considers external and internal temperature variations over multiple cycles and their effects on capacitance evolution and degradation. The model estimating the degree of mass dissolution and degradation and increases in resistance based on the temperature and other operating conditions at each cycle with uncertainty based on the inputs of to the model. Bayesian updating was employed to improve the physics-based model, incorporating experimental and statistical data with uncertainties to enhance its predictive capabilities for real operating conditions. Experimental studies both provided data and helped validate the model's accuracy. This represents the first attempt at modeling the cycling behavior of pseudocapacitors through cyclic voltammetry, which allows additional analysis of the reactions taking place in the material. Further the was the first cyclic model that sought to account for the evolution in internal temperature due to reversible and irreversible heat, connecting it to the degradation of the material species over cycling.

Furthermore, this research demonstrated the applicability of a Bayesian Monte Carlo approach to estimating the remaining useful life (RUL) of pseudocapacitors. By forecasting RUL, this approach can optimize the operation and management of pseudocapacitor energy storage systems, contributing to efficient utilization, reduced downtime, and minimized risk of system failure. This research presents a new approach to predict pseudocapacitor performance, offering insights into reliability and efficiency in energy storage systems for sustainable and dependable power solutions.

7.1. Conclusions and Outlook

In conclusion, this dissertation has made significant strides in understanding and addressing the degradation mechanisms impacting the performance and reliability of MnO2 pseudocapacitors. Through a comprehensive approach encompassing experimental studies, modeling, and probabilistic analyses, the research has shed light on and developed a method for capturing the external and internal temperature effects and dissolution of electrode material into the electrolyte as a critical factor influencing capacitance reduction over numerous cycles. The developed physics-based model stands as a noteworthy achievement, providing a simulation tool capable of capturing capacitance and degradation behaviors over time. This is especially useful for EDLCs and other pseudocapacitors that can have prohibitively long experimental test times for assessing cycle life.

The utilization of Bayesian updating in refining the physics-based model has demonstrated a novel approach to incorporating uncertainties and improving the model ability to reflect reality.

This integration of experimental and statistical data, as well as validation with real data, has elevated the model's ability to predict pseudocapacitor performance, especially under dynamic and unpredictable environmental conditions.

The introduction of a Bayesian Monte Carlo approach for estimating the remaining useful life (RUL) of pseudocapacitors also demonstrates potential to advance the operation, management and lifetime value of larger energy storage systems containing pseudocapacitors. Looking ahead, the findings from this dissertation pave the way for further advancements in the design and implementation of reliable systems that utilize pseudocapacitors for energy storage, such as hybrid battery-pseudocapacitor regenerative braking systems. Future research endeavors could explore additional factors influencing degradation, expand models to encompass broader ranges of operating conditions, and investigate other novel materials for pseudocapacitors. The Bayesian Monte Carlo approach, introduced here for RUL estimation, offers a promising avenue for continued exploration and application in real-world energy storage systems, promising a more sustainable and dependable energy future.

7.2. Future Work: Addressing Model Limitations and Advancing RUL Predictions

The findings of this study have shed light on critical limitations in our RUL prediction model, particularly in accommodating changing environmental conditions such as temperature variations. Several avenues for continued research in this area emerge, each aimed at enhancing the accuracy and adaptability of pseudocapacitor models.

- Uncertainty Analysis of Physics Model Parameters:

One key aspect for future investigation involves a comprehensive analysis of uncertainties associated with parameters in the physics model beyond temperature and active material mass or concentration degradation. Understanding and quantifying uncertainties in parameters such as the changing diffusion parameters, the changing overpotential, the changing charge transfer rates, and others can contribute to a more robust prediction model, especially under dynamic operating conditions.

- Regression Techniques and Criteria for Convergence of Degradation Model Parameters:

To improve the reliability of the degradation model used to predict RUL, it is imperative to define criteria for convergence when fitting the model to real-world data. This involves a systematic exploration of various datasets to ensure the model's adaptability across different operational scenarios. Testing against multiple datasets will validate the model's convergence criteria and enhance its generalizability. Further, exploration of Bayesian regression for fitting the model parameters may be an alternative avenue for refining the RUL prediction. The model currently uses a multiple linear regression technique. A Bayesian regression can better handle uncertainties that may be better suited to available data and potentially improve the predictions of the model. As an extension of this, incorporating Bayesian model uncertainty into the RUL prediction framework can leverage the data to continually refine and tune the model, reducing prediction errors and enhancing the adaptability to changing conditions.

- System-Level Modeling and Experimental Data Integration:

The application of RUL prediction models to system-level modeling is a critical step towards real-world implementation. Future work on this subject will aim to integrate experimental data, such as the self-discharge characteristics of pseudocapacitors obtained in this study, into the

modeling framework. This will allow for a more comprehensive understanding of system behavior and provide practical insights for system-level RUL predictions. For example, understanding the impact of self-discharge on the performance and life of a pseudocapacitor can allow one to optimize, for example, how the current is maintained during charge and discharge of the device when braking and accelerating an electric vehicle with regenerative braking capabilities. As a hybrid battery-supercapacitor system, a battery relieved of these high current loads in a given driving cycle may then experience extended lifetime, increasing the lifetime value of the whole system.

In summary, the future work outlined above seeks to address the identified limitations and elevate the state-of-the-art in RUL prediction models. By delving into uncertainty analysis, convergence criteria, Bayesian regression, and system-level applications, a future model may not only accurate under varying conditions but also adaptable to the complex and dynamic nature of real-world operational environments. These advancements will contribute significantly to the field of prognostics and facilitate the practical implementation of RUL prediction models in diverse industries and applications.

References

[1] IEA, "Global EV Outlook 2023," IEA, Paris, 2023. [Online]. Available: https://www.iea.org/reports/global-ev-outlook-2023,. [Accessed Dec 2023].

[2] Pew, "America's Electric Grid: Growing Cleaner, Cheaper and Stronger," Pew Charitable Trusts, 2015.

[3] P. Forouzandeh, V. Kumaravel and S. C. Pillai, "Electrode Materials for Supercapacitors: A Review of Recent Advances," *Catalysts,* vol. 10, no. 9, p. 969, 2020.

[4] A.T. Kearney Energy Transition Institute, "Hydrogen-based energy conversion," A.T. Kearney, 2014.

[5] N. M. Jamadar and H. Jadhav, "Effectiveness of supercapacitor during braking operation of electric vehicle," *Materials Today: Proceedings,* vol. 56, 2022.

[6] X. Wang, K. Liu, J. Li, Y. Liu, M. Wang and H. Cui, "Creation of an extrinsic pseudocapacitive material presenting extraordinary cycling-life with the battery-type material Co(OH)2 by S2− doping for application in supercapacitors," *Chem. Eng. J,* vol. 451, p. 138969, 2023.

[7] S. Fleischmann, J. B. Mitchell, R. Wang, C. Zhan, D.-e. Jiang, V. Presser and V. Augustyn, "Pseudocapacitance: From Fundamental Understanding to High Power Energy Storage Materials," *Chem. Rev.,* vol. 120, no. 14, pp. 6738-6782, 2020.

[8] C. Choi, D. S. Ashby, D. M. Butts, R. H. DeBlock, Q. Wei, J. Lau and B. Dunn, "Achieving high energy density and high power density with pseudocapacitive materials," *Nature Reviews Materials,* vol. 5, pp. 5-19, 2020.

[9] Y. Cai, R. Chua, S. Huang, H. Ren and M. Srinivasan, "Amorphous manganese dioxide with the enhanced pseudocapacitive performance for aqueous rechargeable zinc-ion battery," *Chemical Engineering Journal,* vol. 396, 2020.

[10] https://pubs.acs.org/action/getFTRLinkout?url=https%3A%2F%2Fct.prod.getft.io%2FYWNzLGVsc2V2aWVyLGh0dHBzOi8vd3d3LnNjaWVuY2VkaXJlY3QuY29tL3NjaWVuY2UvYXJ0aWNsZS9waWkvUzAzNzg3NzUzMTEwMjI5MDc_cGVzPXZvcg.Fndx48S3ZJG52Lfl8iP1YMnZKcy61rpPDgRESia_3ps&doi=10.1021%2.

[11] X. Chen, Y. Wu and R. Holze, "Ag(e)ing and Degradation of Supercapacitors: Causes, Mechanisms, Models and Countermeasures," *Molecules,* vol. 28, no. 13, 2023.

[12] E. Pameté, L. Köps, F. A. Kreth, S. Pohlmann, A. Varzi, T. Brousse, A. Balducci and V. Presser, "The Many Deaths of Supercapacitors: Degradation, Aging, and Performance Fading," *Advanced Energy Materials,* 2023.

[13] S. Liu, L. Wei and H. Wang, "Review on reliability of supercapacitors in energy storage applications," *Applied Energy,* vol. 278, 2020.

[14] M. Ayadi, B. Briat, R. Lallemand, A. Eddahech, R. German, G. Coquery and J. Vinassa, "Description of supercapacitor performance degradation rate during thermal cycling under constant voltage ageing test.," *Microelectron. Reliab.* , pp. 1944-1948, 2014.

[15] T. Liu and Y. Li, "Addressing the Achilles' heel of pseudocapacitive materials: Long-term stability," *InfoMat,* vol. 2, no. 5, pp. 807-842, 2020.

[16] D. Kim, S. Park, O. B. Chae, J. H. Ryu, Y.-U. Kim, R.-Z. Yin and S. M. Oh, "Re-Deposition of Manganese Species on Spinel LiMn2O4 Electrode after Mn Dissolution," *Journal of The Electrochemical Society,* vol. 159, 2011.

[17] http://lu.engin.umich.edu/wp-content/uploads/sites/347/2017/12/15JPSShin-ds.pdf.

[18] C. Zhan, T. Wu, J. Lu and K. Amine, "Dissolution, migration, and deposition of transition metal ions in Li-ion batteries exemplified by Mn-based cathodes – a critical review," *United States: N. p.,,* vol. doi:10.1039/c7ee03122j., 2017.

[19] H. Shin, J. Park, A. M. Sastry and W. Lu, "Degradation of the solid electrolyte interphase induced by the deposition of manganese ions," *Journal of Power Sources,* 2015.

[20] X. Yang, Z. Qiao, F. Liu, S. Yang, L. Zhang and B. C. , "In-depth study of electrochemical capacitor performance of MnO2 during phase transition from Ramsdellite-MnO2 to Birnessite-MnO2," *Electrochimica Acta,* 2018.

[21] https://pubs.acs.org/action/getFTRLinkout?url=https%3A%2F%2Fct.prod.getft.io%2FYWNzLGVsc2V2aWVyLGh0dHBzOi8vd3d3LnNjaWVuY2VkaXJlY3QuY29tL3NjaWVuY2UvYXJ0aWNsZS9waWkvUzAwMTM0Njg2MDgwMTI1MDQ_cGVzPXZvcg.3h2J4L2iIuTMxaUabm0vCNEH4JtD1zP-eogDiBS19qg&doi=10.1021%2.

[22] https://pubs.acs.org/action/getFTRLinkout?url=https%3A%2F%2Fct.prod.getft.io%2FYWNzLGVsc2V2aWVyLGh0dHBzOi8vd3d3LnNjaWVuY2VkaXJlY3QuY29tL3NjaWVuY2UvYXJ0aWNsZS9waWkvUzAwMTM0Njg2MTEwMTY4ODQ_cGVzPXZvcg.x_iJ_Trzsn2n3urOtJ5gXDo_Elelp_wjFEXCji5E5N0&doi=10.1021%2.

[23] S. Han, S. Park, S.-H. Yi, W. B. Im and S.-E. Chun, "Effect of potential and current on electrodeposited MnO2 as a pseudocapacitor electrode: Surface morphology/chemistry and stability," *Journal of Alloys and Compounds,* vol. 831, 2020.

[24] https://pdf.sciencedirectassets.com/271367/1-s2.0-S0378775300X02613/1-s2.0-S0378775304004860/main.pdf?X-Amz-Security-Token=IQoJb3JpZ2luX2VjELr%2F%2F%2F%2F%2F%2F%2F%2F%2F%2FwEaCXVzLWVhc3QtMSJHMEUCIDWBCCsv.

[25] I. S. Ike, I. Sigalas and S. Iyuke, "Understanding performance limitation and suppression of leakage current or self-discharge in electrochemical capacitors: a review," *Physical chemistry chemical physics,* no. 2, 2016.

[26] W. Zhou, Z. Liu, W. C. X. S. M. Luo, X. Zhang, C. Li, Y. An, S. Song, K. W. and X. Zhang, "A Review on Thermal Behaviors and Thermal Management Systems for Supercapacitors," *Batteries,*

2023.

[27] J.-l. Hong, J.-h. Liu, X. Xiong, S.-y. Qin, X.-y. Xu, X. Meng, K. Gu, J. Tang and D.-Z. Chen, "Temperature-dependent pseudocapacitive behaviors of polyaniline-based all-solid-state fiber supercapacitors," *Electrochemistry Communications,* vol. 148, 2023.

[28] T. c. a. p. i. o. a. h. supercapacitor, "Wanqi Liu;Cong Dong; Bo Zhang ; Ruibing Cao ; Zhijun Qiao ; Yuanjun Tang ; Chao Ye ; Ke Li ;Yanghui Ye," *Journal of Energy Storage,* vol. 53, 2022.

[29] M. Teuber, *LIfetime Assessment and Degradation Mechanisms of Electric Double-Layer Capacitors,* Aachen: ISEA. Dissertation., 2019.

[30] N. Ma, D. Yang, L. Wang and K. Wang, "Aging Mechanism and Models of Supercapacitors: A Review," *Technologies,* vol. 11, no. 38, 2023.

[31] L. Zhang, X. Hu, Z. Wang, F. Sun and D. G. Dorrell, "A review of supercapacitor modeling, estimation, and applications: A control/management perspective," *Renewable and Sustainable Energy Reviews,* vol. 81, pp. 1868-1878, 2018.

[32] F. Naseri, S. Karimi, E. Farjah and E. Schaltz, "Supercapacitor management system: A comprehensive review of modeling, estimation, balancing, and protection techniques," *Renewable and Sustainable Energy Reviews,* vol. 155, p. 111913, 2022.

[33] D. A. Bograchev, Y. M. Volfkovich and S. Martemianov, "Diagnostics of supercapacitors using cyclic voltammetry: Modeling and experimental applications," *Journal of Electroanalytical Chemistry,* vol. 935, 2023.

[34] L. Pilon, H. Wang and A. d'Entremont, "Recent Advances in Continuum Modeling of Interfacial and Transport Phenomena in Electric Double Layer Capacitors," *J. Electrochem. Soc.,* vol. 162, 2015.

[35] A. d'Entremont and L. Pilon, "First-principles thermal modeling of electric double layer capacitors under constant-current cycling," *Journal of Power Sources,* vol. 246, pp. 887-898, 2014.

[36] H. Wang and L. Pilon, "Mesoscale modeling of electric double layer capacitors with three-dimensional ordered structures," *Journal of Power Sources,* 2013.

[37] B.-A. Mei and L. Pilon, "Three-Dimensional Cyclic Voltammetry Simulations of EDLC Electrodes Made of Ordered Carbon Spheres," *Electrochimica Acta,* vol. 255, pp. 168-178, 2017.

[38] H.-L. Girard, B. Dunn and L. Pilon, "Simulations and Interpretation of Three-Electrode Cyclic Voltammograms of Pseudocapacitive Electrodes," *Electrochimia Acta,* vol. 211, pp. 420-429, 2016.

[39] H.-L. Girard, H. Wang, A. d'Entremont and L. Pilon, "Physical Interpretation of Cyclic Voltammetry for Hybrid Pseudocapacitors," *J. Phys. Chem. C,* vol. 119, no. 21, pp. 11349-11361, 2015.

[40] H.-L. J.-P. Girard, *Modeling and Physical Interpretation of CyclicVoltammetry for*

Pseudocapacitors (dissertation), 2015.

[41] B.-A. Mei, B. Li, J. Lin and L. Pilon, "Multidimensional Cyclic Voltammetry Simulations of Pseudocapacitive Electrodes with a Conducting Nanorod Scaffold," *J. Electrochem. Soc.*, vol. 164, no. 13, pp. A3237-A3252, 2017.

[42] S. Aderyani, P. Flouda, S. Shah, M. Green, J. Lutkenhaus and H. Ardebili, "Simulation of cyclic voltammetry in structural supercapacitors with pseudocapacitance behavior," *Electrochimica Acta*, vol. 390, 2021.

[43] N. Keilbart, Y. Okada, A. Feehan, S. Higai and I. Dabo, "Quantum-continuum simulation of the electrochemical response of pseudocapacitor electrodes under realistic conditions," *Phys. Rev. B*, vol. 95, 2017.

[44] M. R. Hasyim and R. Rajagopalan, "Prediction of Discharge Performances of Pseudocapacitors Using Their Impedance Characteristics," *J. Electrochem. Soc.*, vol. 167, no. 1, 2020.

[45] G. G. Carvalho, S. Eugénio, M. T. Silva and M. F. Montemor, "Simulation of the Electrochemical Response of Cobalt Hydroxide Electrodes for Energy Storage," *Batteries*, vol. 8, no. 4, 2022.

[46] K. Chatterjee, S. Basu and N. Gupta, "Modelling of an electrochemical double layer capacitor using cyclic voltammetry," in *IEEE Electrical Insulation Conference*, Denver, 2021.

[47] M. W. Verbrugge, P. Liu and S. Soukiazian, "Activated-carbon electric-double-layer capacitors: electrochemical characterization and adaptive algorithm implementation," *Journal of Power Sources*, vol. 141, no. 2, pp. 369-385, 2005.

[48] T. Omori, M. Nakanishi and D. Tashima, "Modeling of Equivalent Circuit Analysis of Degraded Electric Double-Layer Capacitors," *Materials (Basel)*, vol. 14, no. 2, 2021.

[49] M. Kroupa, G. J. Offer and J. Kosek, "Modelling of Supercapacitors: Factors Influencing Performance," *J. Electrochem. Soc.*, vol. 163, 2016.

[50] W. Lin, W. Shen and G. Lou, "(Preprint) State of Health Estimation for Supercapacitors Based on Deep Learning Networks and Bayesian Optimization," *SSRN*, 2022.

[51] D. Roman, S. Saxena, J. Bruns, R. Valentin, M. Pecht and D. Flynn, "A Machine Learning Degradation Model for Electrochemical Capacitors Operated at High Temperature," *IEEE Access*, 2021.

[52] A. Likitchatchawankuna, R. DeBlock, G. Whang, O. Munteshari, M. Frajnkovič, B. Dunn and L. Pilon, "Heat generation in electric double layer capacitors with neat and diluted ionic liquid electrolytes under large potential window between 5 and 80◦C," *Journal of Power Sources*, vol. 488, 2021.

[53] A. Ayob, S. Ansari, M. Shahadat Hossain Lipu, A. Hussain and M. H. M. Saad, "SOC, SOH and RUL Estimation for Supercapacitor Management System: Methods, Implementation Factors, Limitations and Future Research Improvements," *Batteries*, vol. 8, no. 10, p. 189, 2022.

[54] H. L. Y. Z. Liqiang Mai, L. Xu, X. Xu, Y. Luo, Z. Zhang, W. Ke, C. Niu and Q. Zhang, "Fast Ionic Diffusion-Enabled Nanoflake Electrode by Spontaneous Electrochemical Pre-Intercalation for High-Performance Supercapacitor," *Nature, Scientific Reports,* 2013.

[55] W. M. Dose and S. W. Donne, "Thermal Treatment Effects on Manganese Dioxide Structure, Morphology and Electrochemical Performance," *Journal of The Electrochemical Society,* vol. 158, 2011.

[56] B. Deljoo, H. Tan, S. L. Suib and M. Aindow, "Thermally activated structural transformations in manganese oxide nanoparticles under air and argon atmospheres," *Journal of Materials Science,* vol. 55, pp. Bahareh Deljoo, Haiyan Tan, Steven L. Suib & Mark Aindow, 2020.

[57] H. Chen, S. Zenga, M. Chen, Y. Zhanga and Q. Li, "A new insight into the rechargeable mechanism of manganese dioxide based symmetric supercapacitors," *RSC Adv.*, vol. 7, pp. 8561-8566, 2017.

[58] S. Han, S. Park, S.-H. Yi, W. B. Im and S.-E. Chun, "Effect of potential and current on electrodeposited MnO2 as a pseudocapacitor electrode: Surface morphology/chemistry and stability," *Journal of Alloys and Compounds,* vol. 831, 2020.

[59] S. Pappu, T. N. Rao, S. K. Martha and S. V. Bulusu, "Electrodeposited Manganese Oxide based Redox Mediator Driven 2.2 V High Energy Density Aqueous Supercapacitor," *Energy ,* 2022.

[60] D. Cornu, R. Coustel, G. Renaudin, G. Rogez, A. Renard, P. Durand, C. Carteret and C. Ruby, "Synthesis and characterization of a new monometallic layered double hydroxide using manganese," *Dalton Transactions,* no. 31, 2022.

[61] T. Takashima, K. Hashimoto and R. Nakamura, "Mechanisms of pH-Dependent Activity for Water Oxidation to Molecular Oxygen by MnO2 Electrocatalysts," *J.Am.Chem.Soc.*, vol. 134, pp. 1519-1527, 2012.

[62] L.-F. Wang, C.-C. Ou, K. A. Striebel and J.-S. Chen, "Study of Mn dissolution from LiMn2O4 spinel electrodes using rotating ring-disk collection experiments," *Journal of The Electrochemical Society,* vol. 150, no. 7, 2003.

[63] Y. Liu, Z. Qin, X. Yang and X. Sun, "A Long-Life Manganese Oxide Cathode Material for Aqueous Zinc Batteries with a Negatively Charged Porous Host to Promote the Back-Deposition of Dissolved Mn2+," *Advanced Functional Materials,* vol. 32, no. 10, 2021.

[64] S. B. Aziz, M. A. B. I. Brevik, M. H. Hafiz, A. S. Asnawi, Y. M. Yusof, R. T. Abdulwahid and M. F. Kadir, "Blending and Characteristics of Electrochemical Double-Layer Capacitor Device Assembled from Plasticized Proton Ion Conducting Chitosan:Dextran:NH4PF6 Polymer Electrolytes," *Polymers,* vol. 12, no. 9, 2013.

[65] J. Wang, Z. Zhao, S. Song, Q. Ma and R. Liu, "High Performance Poly(vinyl alcohol)-Based Li-Ion Conducting Gel Polymer Electrolyte Films for Electric Double-Layer Capacitors," *Polymers,* vol. 10, no. 11, 2018.

[66] [Online]. Available: https://www.sciencedirect.com/science/article/pii/S0013468620301948#fig1.

[67] Z. J. Han, Z. Bo, D. H. Seo, S. Pineda, Y. Wang, H. Y. Yang and K. (. Ostrikov, "High Pseudocapacitive Performance of MnO2 Nanowires on Recyclable Electrodes," *Chem. Sus. Chem,* vol. 9, no. 9, pp. 1020-1026, 2016.

[68] Z. Ren, J. Li, Y. Ren, S. Wang, Y. Qiu and J. Yu, "Large-scale synthesis of hybrid metal oxides through metal redox mechanism for high-performance pseudocapacitors," *Nature Scientific Reports,* vol. 6, 2016.

[69] J. Kang, A. Hirata, H.-J. Qiu, L. Chen, X. Ge, T. Fujita and M. Chen, "Self-Grown Oxy-Hydroxide@ Nanoporous Metal Electrode for High-Performance Supercapacitors," *Advanced Materials,* vol. 26, no. 2, pp. 269-272, 2014.

[70] G. Tazwar and V. Devra, "Soluble Colloidal Manganese Dioxide: Formation, Characterization and Application in Oxidative Kinetic Study of Ciprofloxacin," *BCREC,* vol. 15, no. 1, pp. 74-83, 2020.

[71] Islam and Rahman, "Soluble Colloidal Manganese Dioxide: Formation, Identification and Prospects of Application," *Colloidal Journal,* vol. 75, no. 5, pp. 591-595, 2013.

[72] S. Saha, "Zinc iron phosphate glasses for enameling applications," *Master's thesis. Missouri S&T,* 2010.

[73] S. Sopcic, N. Seselj and M. K. Rokovic, "Influence of supporting electrolyte on the pseudocapacitive properties of MnO2/carbon nanotubes," *Journal of Solid State Electrochemistry,* 2019.

[74] X. Ye, D. Han, G. Jiang, Changjun Cui, .Yong Guo, Yaogang Wang, Z. Zhang, Z. Weng and Q.-H. Yang, "Unraveling the deposition/dissolution chemistry of MnO2 for high-energy aqueous batteries," *Energy and Environ Sci,* no. 3, 2023.

[75] S. Deveraj and N. Munichandraiah, "EQCM investigation of the electrodeposition of MnO2 and its capacitance behavior," *Electrochemical and Solid-State Letters,* 2009.

[76] P. K. Nayak and N. Munichandraiah, "An EQCM investigation of capacitance of MnO2 in electrolytes containing multivalent cations," *Journal of Electroanalytical Chemistry,* vol. 685, 2012.

[77] X. Ye, D. Han, Guangyi Jiang, Changjun Cui, Y. Guo, Yaogang Wang, Z. Zhang, Z. Weng and Q.-H. Yang, "Revealing deposition/dissolution chemistry of MnO2 for high-energy aqueous batteries," *Energy and Environmental Science,* no. 3, 2023.

[78] O. Fitz, C. Bischoff, M. Bauer, H. Gentischer and K. P. Birke, "Electrolyte Study with in Operando pH Tracking Providing Insight into the Reaction Mechanism of Aqueous Acidic Zn//MnO2 Batteries," *Chem Electro Chem,* vol. 8, p. 3553–3566, 2021.

[79] A. Bothe and A. Balducci, "Thermal analysis of electrical double layer capacitors: Present status and remaining challenges," *Journal of Power Sources,* vol. 548, 2022.

[80] P. Guillemet, T. Brousse, O. Crosnier, Y. Dandeville, L. Athouel and Y. Scudeller, "Modeling pseudo capacitance of manganese dioxide," *Electrochimica Acta,* vol. 67, 2012.

[81] R.-B. I. M. o. N. G. P. S. t. S.-T. C. E. (dissertation), *Keo-Yuan Wu,* University of California, Los Angeles, 2020.

[82] J. Schiffer, D. Linzen and D. U. Sauer, "Heat generation in double layer capacitors," *Journal of Power Sources,* vol. 160, no. 1, pp. 756-772, 2006.

[83] Y. Dandeville, P. Guillemet, Y. Scudeller, O. Crosnier, L. Athouel and T. Brousse, "Measuring time-dependent heat profiles of aqueous electrochemical capacitors under cycling," *Thermochimica Acto,* vol. 526, no. 1-2, pp. 1-8, 2011.

[84] X. Zhang, W. Wang, J. Lu, L. Hua and J. Heng, "Reversible heat of electric double-layer capacitors during galvanostatic charging and discharging cycles," *Thermochimica Acta,* vol. 636, pp. 1-10, 2016.

[85] S. Wang, T. Wu, H. Xie, C. Li, J. Zhang, L. Jiang and Q. Wang, "Effects of Current and Ambient Temperature on Thermal Response of Lithium Ion Battery," *Batteries,* vol. 8, no. 11, 2022.

[86] H. Gualous, H. Louahlia and R. Gallay, "Supercapacitor Characterization and Thermal Modelling With Reversible and Irreversible Heat Effect," *IEEE TRANSACTIONS ON POWER ELECTRONICS,* vol. 26, no. 11, 2011.

[87] T. Đukić, L. J. Moriau, L. Pavko, M. Kostelec, M. Prokop, F. Ruiz-Zepeda, M. Šala, G. Dražić, M. Gatalo and N. Hodnik, "Understanding the Crucial Significance of the Temperature and Potential Window on the Stability of Carbon Supported Pt-Alloy Nanoparticles as Oxygen Reduction Reaction Electrocatalysts," *ACS Catalysis,* vol. 12, no. 1, pp. 101-115, 2022.

[88] P. K. Nayak and N. Munichandraiah, "An EQCM investigation of capacitance of MnO2 in electrolytes containing multivalent cations," *Journal of Electroanalytical Chemistry,* vol. 685, pp. 37-40, 2012.

[89] K. Goebel, B. Saha, A. Saxena, J. R. Celaya and J. P. Christopherson, "Prognostics in Battery Health Management," IEEE Instrumentation & Measurment Magazine, 2008.

[90] B. Saha, K. Goebel, S. Poll and J. Christophersen, "Prognostics Methods for Battery Health Monitoring Using a Bayesian Framework," *IEEE TRANSACTIONS ON INSTRUMENTATION AND MEASUREMENT,* vol. 58, no. 2, 2009.

[91] T. Dong, D. An and K. N. H., "Prognostics 102: Efficient Bayesian-Based Prognostics Algorithm in MATLAB," in *Prognostics,* IntechOpen.

[92] Abassi, 2022.

[93] D. Kaplan, "On the Quantification of Model Uncertainty: A Bayesian Perspective," *Psychometrika,* vol. 86, pp. 215-238, 2021.

[94] E. L. Droguett and A. Mosleh, "Bayesian Treatment of Model Uncertainty for Partially Applicable

Models," *Risk Analysis,* 2013.

[95] US EPA, "Dynamometer Drive Schedules," EPA, 4 October 2023. [Online]. Available: https://www.epa.gov/vehicle-and-fuel-emissions-testing/dynamometer-drive-schedules.

[96] A. Yu, V. Chabot and J. Zhang, Electrochemical Supercapacitors for Energy Storage and Delivery, Boca Raton: Taylor & Francis Group, 2013.

[97] H. Shin, J. Park, A. M. Sastry and W. Lu, "Degradation of the solid electrolyte interphase induced by the deposition of manganese ions," *Journal of Power Sources,* vol. 28, no. 15, pp. 416-426, 2015.

[98] X. Chen, Y. W. and R. Holze, "Ag(e)ing and Degradation of Supercapacitors: Causes, Mechanisms, Models and Countermeasures," *Molecules,* 2023.